Journal of Medicinal Chemistry

pubs.acs.org/jmc

Article

Small Molecule–Degrader Conjugates: Evaluating the Structure–Activity Relationship of Linkers to Overcome In Vivo Barriers in PROTAC Delivery

Shiwei Song, Weina Jing, Lei Peng, Jiaqi Liu, and Wanyi Tai*

Cite This: https://doi.org/10.1021/acs.jmedchem.5c00862

Read Online

ACCESS | Metrics & More | Article Recommendations | Supporting Information

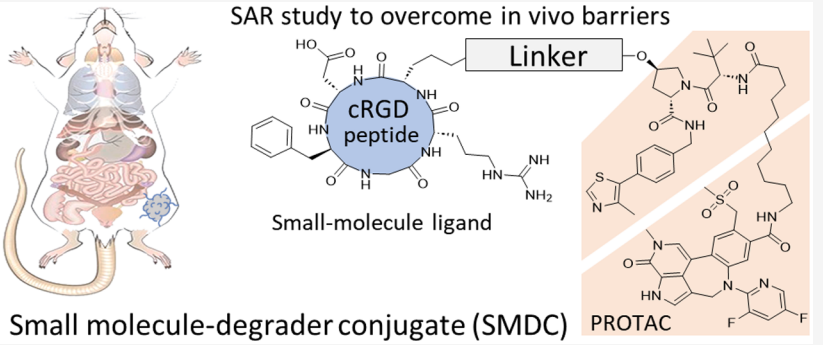

ABSTRACT: Precise control of proteolysis on target cells is important for proteolysis-targeting chimeras (PROTAC) to minimize off-tissue toxicities. Small-molecule ligand-guided PROTACs, namely, small molecule–degrader conjugates (SMDCs), offer many advantages, but some flaws in the previous designs, especially linker chemistry, cause a considerable defect in pharmacokinetics, which impedes in vivo applications. Here, we investigated the relationship of linker structures with in vivo factors, including serum stability, blood retention, controlled PROTAC release, targetability, and potency. Based on the structure–activity relationship (SAR) study, the cathepsin-responsive/carbamate linker bearing a long-circulating CBB protractor was developed to conjugate the cRGD peptide and GNE-987 PROTAC. This peptide-drug conjugate showed an excellent targeting capability, long-term stability, and favorable pharmacokinetics, which enabled the selective proteolysis of targets in an antigen-dependent manner and achieved a tumor growth arrest in vivo by a dose much lower than regular SMDCs and free PROTACs. Our results demonstrated that linker-optimized SMDC degraders can be promising modalities in precision medicine.

INTRODUCTION

Proteolysis-targeting chimera (PROTAC) is a new class of therapeutic modalities that induces the target protein degradation by hijacking the ubiquitin proteasome system (UPS).[1] They are generally heterobifunctional molecules composed of two active ligands: one binds to a protein of interest (POI), while the other selectively engages an E3 ubiquitin ligase. The recruitment of the E3 ligase to the POI by PROTAC molecules triggers a polyubiquitination process and ultimately leads to the proteasome-mediated degradation of POI.[2,3] Compared to the traditional occupancy-based inhibitors, PROTAC offers numerous advantages including (i) a catalytic nature enabling stoichiometric elimination of POI; (ii) degradation of target proteins instead of inhibition, potentiating the pharmacological effect; and (iii) a wide range of targets including the "undruggable" and "non-enzymatic" proteins.[1,4] These exciting features make PROTAC extremely powerful in manipulating disease-relevant pathways. Some PROTAC molecules, such as GNE-987 targeting BRD4 via VHL E3 ligase, can exhibit picomolar activity (DC_{50} = 0.03 nM) and near-complete protein degradation (D_{max} = 99%) in cancer cell lines, making them extremely popular in drug discovery.[5,6]

Despite high activity, these reported PROTACs are not tissue-specific. Most PROTACs recruit endogenous E3 ligases for target proteolysis. These ligases, covering a family of over 600 members, are broadly expressed in many tissues and organs.[7] Some PROTACs were reported to recruit organ-specific E3 ligases for more cell-type-selective degradation.[8,9] However, spatial distribution and potential off-tissue effects after systemic administration may lead to the uncontrolled degradation, even toxicity, in normal tissues, limiting the

Received: March 27, 2025
Revised: August 1, 2025
Accepted: August 7, 2025

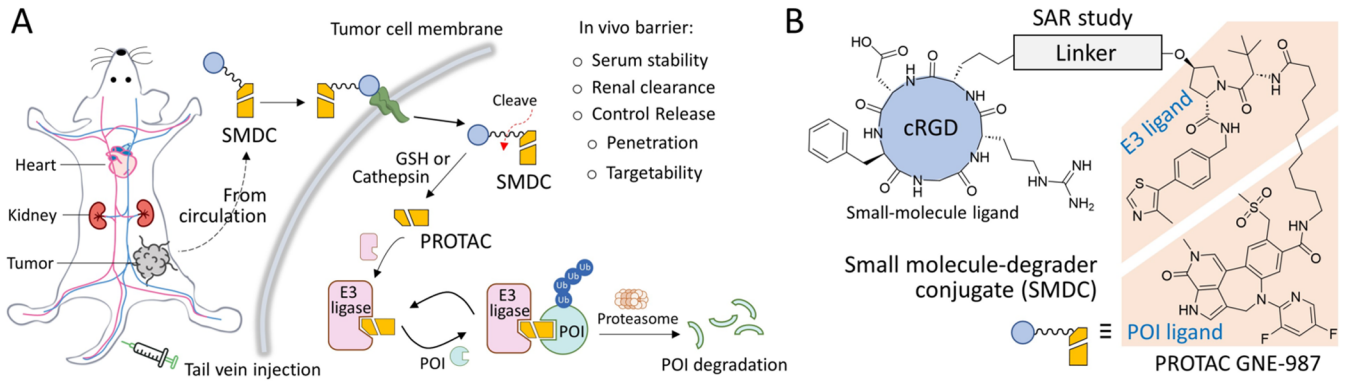

Figure 1. Schematic diagram showing the mode of action of small-molecule ligand-guided PROTAC degrader SMDCs. (A) PROTAC delivery from the injection site to the tumor-cell UPS machinery by SMDCs. SMDCs need to overcome a series of in vivo barriers, which poses a high requirement to the chemistry and functions of SMDC linkers. (B) The SAR study of SMDC linkers to improve the serum stability, pharmacokinetics, site-specific release, and potency.

therapeutic window in the clinic. In this regard, the targeted delivery has become an important strategy in the PROTAC therapy.[6,10] Antibody-conjugated PROTACs, known as degrader-antibody conjugates (DACs), have been developed for the targeted delivery, for example, BRD4-targeting DAC, ERα-targeting DAC, TGFβR2-targeting DAC, and BRM-targeting DAC.[11−14] However, their application is hindered by some limitationsincluding the payload-induced instability, high molecular weight, and poor penetration after systemic administration, which have been discussed in many reviews.[15,16] Besides antibody, small-molecule ligand is another type of tumor-homing ligand that can conjugate with PROTACs for targeted delivery. Small-molecule ligands, such as folic acid, DUPA, and cyclic peptides, are well established in the clinical setting for tumor imaging and therapy.[17−19] Compared to antibodies, small-molecule ligands have more compact sizes, which endow PROTACs with numerous benefits such as low manufacturing cost, deep penetration, and good immune tolerance.[20] Prof. Wei and other laboratories have independently reported two small-molecule ligand-conjugated PROTACs using folic acid and iRGD.[21,22] These *s*mall *m*olecule−*d*egrader *c*onjugates, referred to henceforth as SMDC, achieve the targeted degradation of POI in cancer cells in vitro, but their efficacy is inferior in animal studies. The poor performance in vivo could be attributed to the unstable ester linkage and extremely short half-life in the circulation, which prevents the gradual accumulation of PROTACs in tumors and impairs the in vivo efficacy. This drawback is also seen in other small-molecule-based conjugates and has led to the failure of Vintafolide, a folic acid-based drug conjugate terminated in phase 3 clinical trial.[23,24] The linker of SMDC plays vital roles in balancing the stability of SMDC in circulation and its lability for activation at tumor sites. Although it shares many commonalities with the linkers of DACs, the design of SMDC linkers should consider other settings, such as conjugation chemistry with small-molecule ligands, renal clearance rate, and stabilities, which requires a systemic investigation.

This study aims to develop a potent and long-circulating SMDC degrader by exploring the structure−activity relationship (SAR) of SMDC linkers (Figure 1A). We chose cyclic RGD (cRGD) as a model ligand and GNE-987 as a PROTAC. Ligand cRGD is a cyclic pentapeptide that can specifically bind $\alpha_v\beta_3$ integrin receptors. When linked with GNE-987, it would guide payloads to the cancer or cancer-relevant cells that overexpress the receptors. These two moieties are conjugated by a diverse array of linker chemistry to investigate serum stability, blood retention, controlled release, and targetability (Figure 1B). We found that the disulfide bond-based carbamate linker is more stable in serum than the carbonate linker. However, SMDC based on both linkers demonstrates a short circulatory half-life and poor pharmacokinetics (PK) owing to the fast renal clearance. By introducing a Coomassie brilliant blue (CBB) protractor, the linker can elongate the SMDC half-life over 12 h in mice without compromise on tumor selectivity. With the increment of blood retention time, the disulfide bond in the linker becomes the limiting factor to SMDC stability in vivo, and a cathepsin-responsive tetrapeptide (GGFG) is selected to replace it for the precise control of PROTAC release in tumor cells. Finally, the SMDC of this linker meets all the requirements, including compact size (3.5 kDa), deep penetration, long circulation half-life, tumor selectivity, stable structure, and controllable PROTAC release, which eventually achieve the tumor-selective and long-term degradation of POI in the mouse xenograft models.

RESULTS AND DISCUSSION

Design and Synthesis of Tumor-Selective PROTAC Conjugates. We first designed small molecule−degrader conjugate version 1 (SMDC1) by employing a disulfide-containing carbonate linker to bridge the tumor-specific cRGD ligand and PROTAC molecule GNE-987 (Figure 1A). The small-molecule ligand cRGD is a well-known cyclic peptide that specifically binds to the cancer-relevant $\alpha_v\beta_3$ integrin receptor.[25] Here, it was chosen as a model ligand and could be easily replaced by other small-molecule ligands to conform with tumors of other biomarkers. To ensure that SMDC itself does not recruit E3 ligase and induce nonspecific degradation, we masked the hydroxyproline of PROTAC by the linker. It was reported that the hydroxyl group of VHL ligand is critical to the binding of E3 ubiquitin ligase.[26] The caging effect to block the PROTAC is temporary and reversible.[5,12] Once uptake by cells, GNE-987 would be released from SMDC by disulfide reduction and subsequent linker self-immolation. In the linker of SMDC1, a sulfonate group was introduced to increase the aqueous solubility; meanwhile, a pendent lysine was added near the disulfide linkage to provide a handle for the

https://doi.org/10.1021/acs.jmedchem.5c00862
J. Med. Chem. XXXX, XXX, XXX−XXX

Scheme 1. Synthesis of Linker-GNE987 7[a]

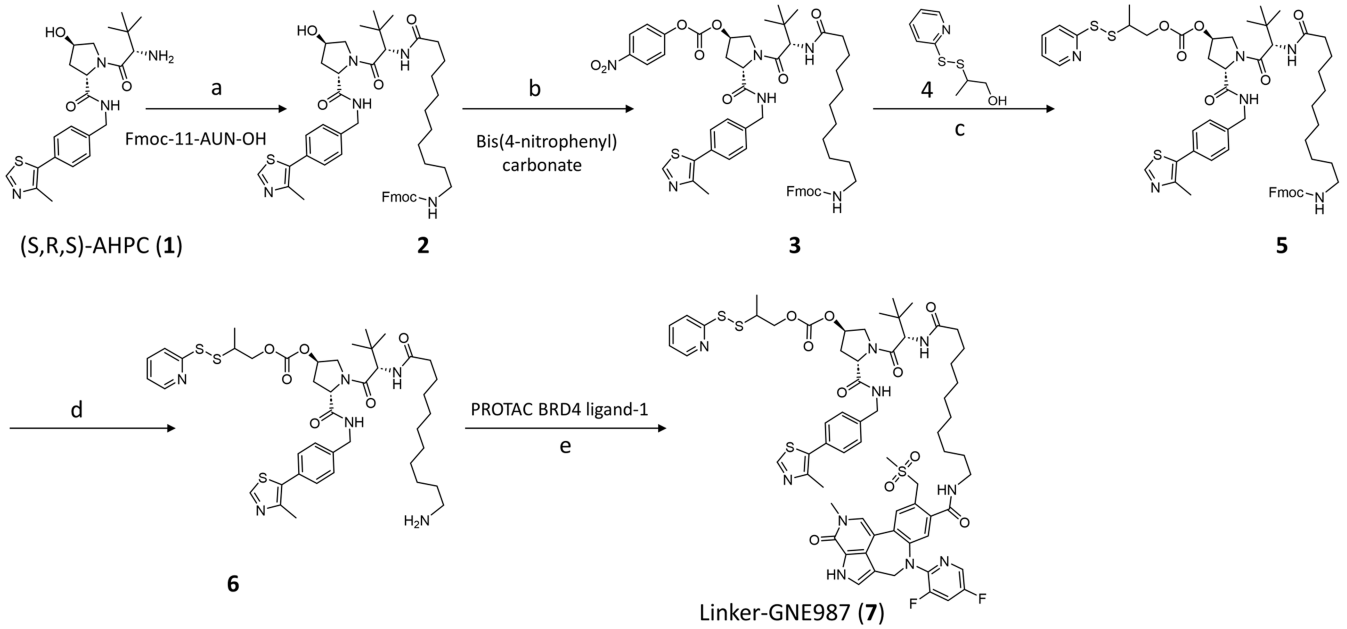

[a]Reaction conditions: (a) Fmoc-11-Aun−OH, hexafluorophosphate azabenzotriazole tetramethyl uronium (HATU), *N*,*N*-diisopropylethylamine (DIPEA), dimethylformamide (DMF), room temperature (rt), 1 h; (b) bis(4-nitrophenyl) carbonate, DIPEA, DMF, rt, 2 h; (c) triethylamine (TEA), dichloromethane (DCM), rt, 3 h; (d) TEA/DMF = 1:5, rt, 4 h; (e) HATU, DIPEA, DMF, rt, 1 h.

Scheme 2. Synthesis of Linker-GNE987 13 and 14[a]

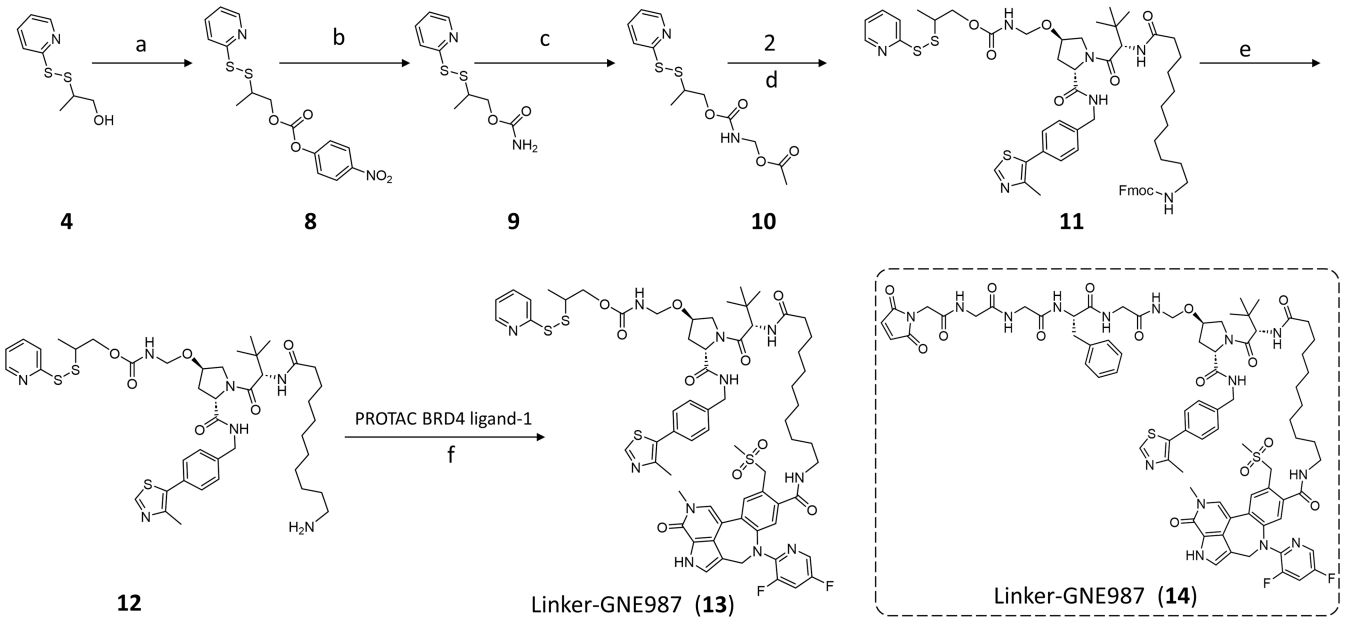

[a]Reaction conditions: (a) bis(4-nitrophenyl) carbonate, DIPEA, DMF, rt, 2 h; (b) NH_3 in 1,4-dioxane, Py, rt, 3 h; (c) paraformaldehyde, acetic acid, 75 °C, 1 h; (d) PPTS, DCM, 40 °C, 24 h; (e) TEA/DMF = 1:5, rt, 4 h; (f) HATU, DIPEA, DMF, rt, 1.5 h.

fluorescent dye conjugation (α-amine) and CBB protractor grafting (ε-amine) in the later design.

The synthesis of SMDCs was achieved by coupling the thiol-activated GNE987 (Linker-GNE987) with the cRGD ligand at the middle of the SMDC linker. This coupling site has a highly reactive thiol group (the cysteine residue) and is also distal from the bulky ends, which can increase the coupling yield. The Linker-GNE987 **7** was synthesized from (*S*,*R*,*S*)-AHPC (**1**) in 5 steps, as shown in Scheme 1. The building block 2-mercaptopropanol was selected to construct the linker because it contains one methyl group around the disulfide bridge and shows an increasing resistance to the cleavage by thiol−disulfide exchange reactions.[27] Synthesis of Linker-GNE987 **13** is shown in Scheme 2, and Linker-GNE-987 **14** was prepared according to our previous report.[28] The cRGD ligand was synthesized following the route described in Scheme 3. The NHS-activated linker **19** or **20** condensed with the lysine residue of cRGD. The intermediate was then deprotected to

https://doi.org/10.1021/acs.jmedchem.5c00862
J. Med. Chem. XXXX, XXX, XXX−XXX

Scheme 3. Synthesis of SMDCs[a]

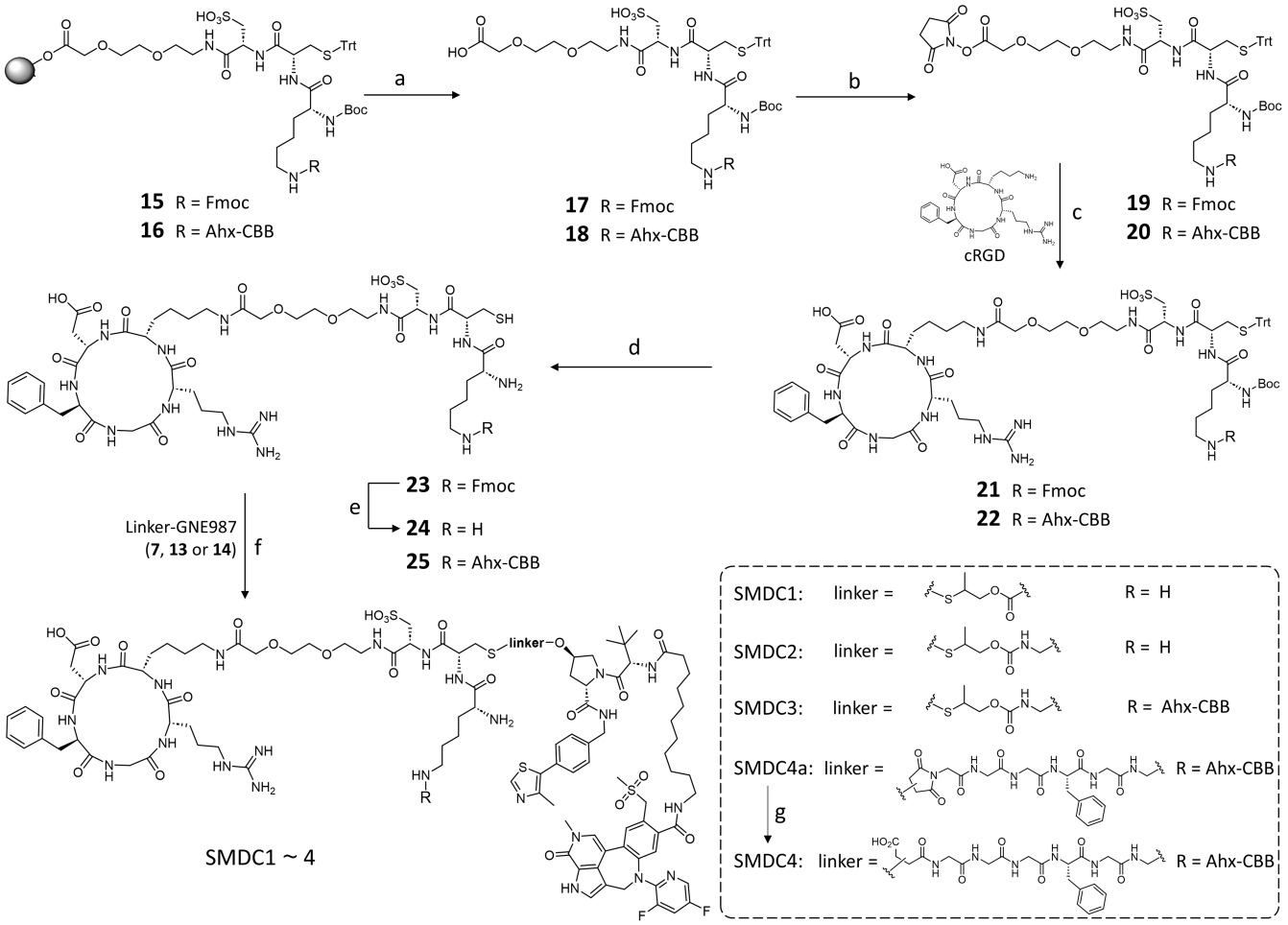

[a]Reaction conditions: (a) AcOH, TFE, DCM, rt, 2 h; (b) 1-ethyl-3-(3-dimethylaminopropyl)carbodiimide (EDCI), HOSu, DMF, rt, 4 h; (c) DIPEA, DMF, rt, 4 h; (d) trifluoroacetic acid (TFA)/DCM = 1:2, rt, 2 h; (e) TEA/DMF = 1:4, rt, 4 h; (f) DMF, rt, 4 h; (g) 0.1 M $NaHCO_3$/DMF (1:1), rt, 5 h.

free the thiol group of cysteine and coupled with Linker-GNE987, producing SMDCs with moderate yields. All of the SMDCs were synthesized in a similar way, but using the different Linker-GNE987 intermediates (Scheme 3). SMDCs were purified by reversed-phase high-performance liquid chromatography (RP-HPLC) and characterized by electrospray ionization (ESI) mass spectrometry.

Serum Stability of the Disulfide-Based Linkers. To this end, we obtained cancer-selective PROTAC (SMDC1). It can selectively bind the $\alpha_v\beta_3$ integrin-positive tumor cells and automatically release the PROTAC payload upon the receptor-mediated cellular uptake (Figure 1A). To test the tandem self-immolation process after disulfide reduction, the SMDC1 was treated by dithiothreitol (DTT, 5 equiv), and the released intermediates were monitored by HPLC. The chromatograms in Figure 2B (first panel) demonstrate that the immolative process occurs instantly after disulfide cleavage. The treated SMDC was converted to GNE-987 in as short as 0.1 h, indicating the high efficiency of PROTAC release. The release process of this SMDC was further evaluated in cancer cells versus normal cells (prostate cancer cell line 22Rv1 and noncancerous prostate cell line RWPE-1). The cell viability in Figure 2A (top right) reveals that SMDC1 is 1000× more potent in 22Rv1 than in RWPE-1 cells. To assess the stability in the bloodstream, we incubated SMDC1 with 90% mouse serum at 37 °C over time and analyzed the degradation by HPLC. The SMDC1 peaks were quickly converted into GNE-987 in as little as 0.5 h (Figure 2B, second panel). Surprisingly, we did not see the semiconjugate1 (sc1) peak that is shown in Figure 2B, first panel, indicating that the cleavage did not occur first at the disulfide bond. Accordingly, we speculated that the instability was likely caused by the fast hydrolysis of carbonate ester linker by the esterase in serum. The ester linkage has been previously described by other groups to conjugate PROTACs with antibodies.[5,12] However, our data indicated that the carbonate linker, despite being stable in cell culture media, is unstable in mouse serum. It led to the linker design of version 2 (SMDC2).

The structure of SMDC2 follows SMDC1, but the carbonate linker is replaced by a carbamate connection (Figure 2A). Carbamate linkage is widely used by ADCs, and its in vivo stability has been well demonstrated in the clinical practice.[29] Upon reductive cleavage, the carbamate linker in this design would undergo a tridem immolating process to release the free GNE-987, as shown in Figure 2A,B (third panel). The stability of SMDC2 in mouse serum was significantly improved, with >70% of intact linker after 8 h at 37 °C (Figure 2B, fourth panel). We also observed that the pendent handle lysine in

https://doi.org/10.1021/acs.jmedchem.5c00862
J. Med. Chem. XXXX, XXX, XXX−XXX

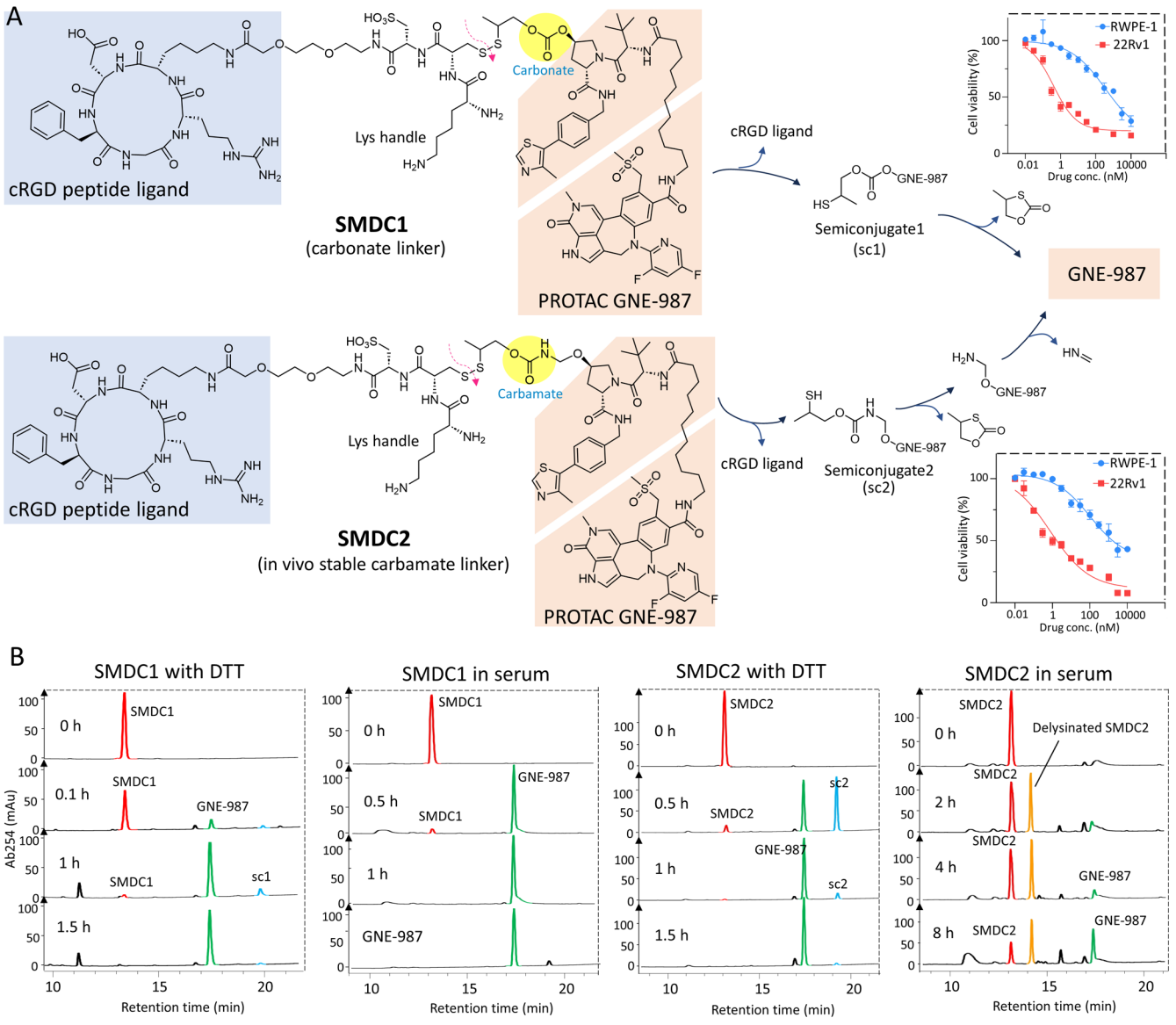

Figure 2. Comparison of the linker stability. (A) Structural comparison of the SMDC1 and SMDC2 linkers. The proposed modes of PROTAC release after reductive cleavage are shown on the right. The dashed red arrows indicate the sites of reductive cleavage. The filled yellow circles highlight the structures of carbonate and carbamate, which differentiate SMDC version 2 and version 1. Their antiproliferation profiles in tumor cells are placed on the top right and bottom right, respectively. (B) HPLC evaluation of SMDC1 and SMDC2 stability in the presence of reductive agent DTT (50 μM) or 90% mouse serum. Note: the yellow peaks in the right panels represent the delysinated SMDC2 (Figure S1).

SMDC2 can be chopped off by the exopeptidase in serum and generate a nascent peak nearby (delysinated SMDC2, Figure S1). Fortunately, the peptide bond can be stabilized by masking the lysine residue with Fmoc or protractor molecules (Figure S2). The SMDC2 was tested on the two cell lines 22Rv1 and RWPE-1 (Figure 2A, bottom right). Its bioactivity in cancerous 22Rv1 cells is as profound as SMDC1, but the cytotoxicity in noncancerous prostate cells RWPE-1 is less prominent than that of SMDC1, indicating a better stability of SMDC2 linker.

Addition of CBB Protractor to Linker Improves Serum Stability and Shows High Potency. The serum-stable linkage encouraged us to incorporate a protractor molecule in the linker for better performance in vivo, referred to as SMDC3 (Figure 3A). In this study, we chose CBB as a protractor, with the assumption that CBB will bind the albumin protein and elongate the retention time in the blood circulation. CBB is a well-known protein staining dye commonly used in biochemistry laboratories. It is also an FDA-approved drug for human use in the retinal surgery under the trade name Brilliant Peel.[30,31] CBB binds noncovalently with protein surface via heteropolar bond and van der Waals forces.[32] The interaction is reversible and applicable to many proteins, including serum albumin. As shown in Figure 3B, SMDC3 exhibits a dramatically improved stability in mouse serum in comparison to its parent SMDC2. The stability improvement is likely attributed to albumin binding, which bulks the size of SMDC and shields the linker against hydrolysis. Meanwhile, we noticed that the recruitment of albumin by CBB slightly attenuated the affinity of SMDC3 to tumor cells (Figure 3C).

To characterize the degrader activity, we treated the $\alpha_v\beta_3$ integrin-positive U87MG cells with 10 nM compounds and assessed protein levels by Western blotting (Figure 3D).

https://doi.org/10.1021/acs.jmedchem.5c00862
J. Med. Chem. XXXX, XXX, XXX−XXX

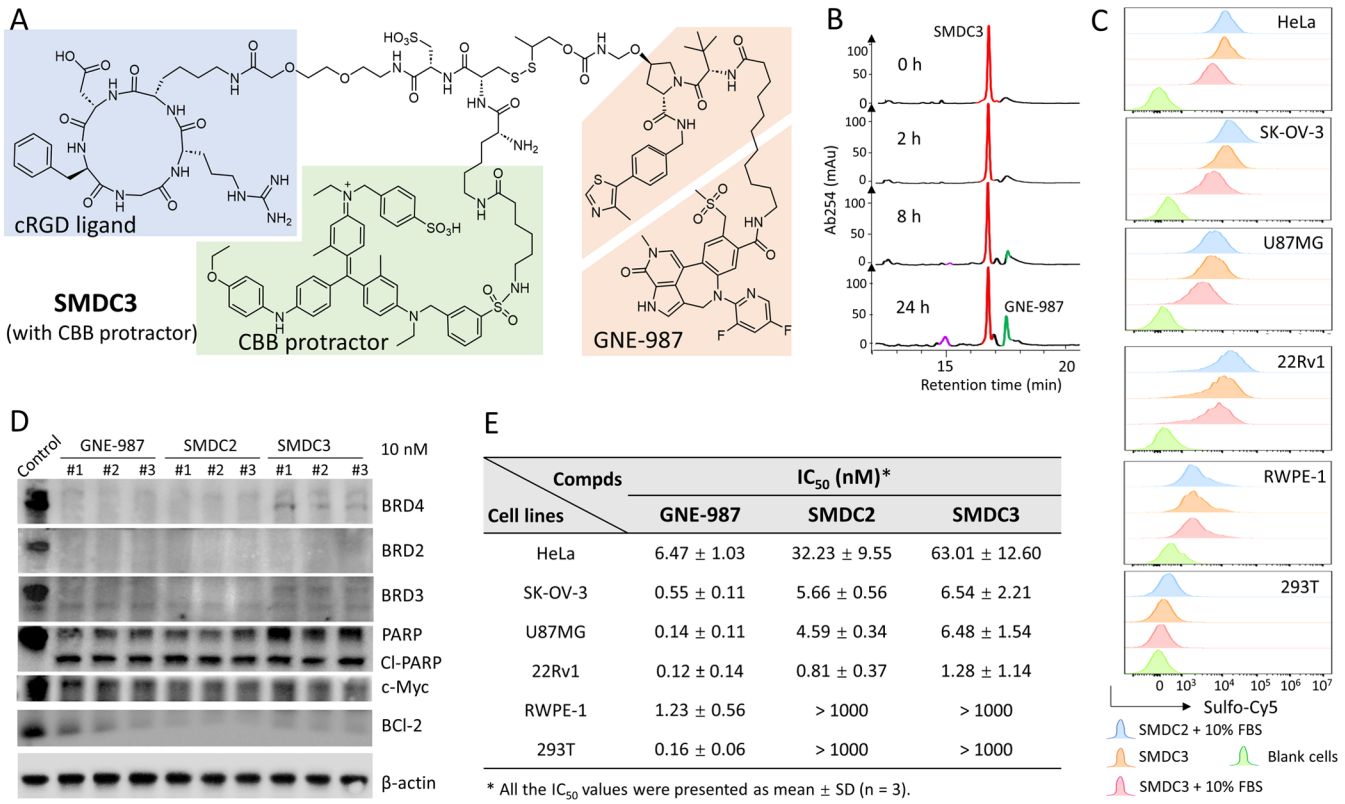

E

Compds / Cell lines	IC$_{50}$ (nM)* GNE-987	SMDC2	SMDC3
HeLa	6.47 ± 1.03	32.23 ± 9.55	63.01 ± 12.60
SK-OV-3	0.55 ± 0.11	5.66 ± 0.56	6.54 ± 2.21
U87MG	0.14 ± 0.11	4.59 ± 0.34	6.48 ± 1.54
22Rv1	0.12 ± 0.14	0.81 ± 0.37	1.28 ± 1.14
RWPE-1	1.23 ± 0.56	> 1000	> 1000
293T	0.16 ± 0.06	> 1000	> 1000

* All the IC$_{50}$ values were presented as mean ± SD (n = 3).

Figure 3. Incorporation of protractor CBB in linker increases the SMDC stability and retains the high potency. (A) Chemical structure of SMDC3. It follows the same scaffold to SMDC2, but a protractor CBB is grafted on the lysine handle of linker. (B) Evaluation of the SMDC3 stability in 90% mouse serum at 37 °C. (C) The parallel charts revealing the impact of fetal bovine serum (FBS) on the binding avidity of SMDC3 to tumor cells. HeLa, SK-OV-3, U87MG, and 22Rv1 are $\alpha_v\beta_3$ integrin-positive cells; RWPE-1 and 293T cells are negative. (D) Western blot analysis of BRD4, BRD2, BRD3, and their downstream proteins in U87MG cells after treatment by GNE-987 (10 nM), SMDC2 (10 nM), and SMDC3 (10 nM). (E) Cytotoxicity assay after 72 h of treatment to determine the IC$_{50}$ values of GNE-987, SMDC2, and SMDC3 in 6 cell lines.

Profound degradation across BET proteins (BRD2, BRD3, and BRD4) was observed in all three treated groups. The proteins downstream of BETs such as c-Myc and BCL-2 were also downregulated.[33,34] Meanwhile, robust cleavage of PARP (Cl-PARP) was observed, indicating the apoptosis induction by all three degraders.[35] In line with the selectivity to the $\alpha_v\beta_3$ integrin, SMDCs elicit cytotoxicity depending on cell types (Figures 3E and S3). For example, SMDC3 is toxic to the $\alpha_v\beta_3$ integrin-expressing cancer cell lines including HeLa cells (IC$_{50}$ 63 nM), SK-OV-3 (IC$_{50}$ 6.54 nM), U87MG cells (IC$_{50}$ 6.48 nM), and 22Rv1 cells (IC$_{50}$ 1.28 nM), but tolerable to the noncancerous normal cell lines 293T (IC$_{50}$ > 1000 nM) and RWPE-1 (IC$_{50}$ > 1000 nM). In contrast, GNE-987 is nonselective and induces toxicity to all cell lines at the low nanomolar range (IC$_{50}$ from 0.12 to 6.47 nM).

Linker-Upgraded SMDC3 Is a Cell-Selective and Long-Circulating Degrader. To assess the cell selectivity, we compared the effect of three degraders on degrading BRD4 in 4 cell lines. As shown in Figure 4A, GNE-987 is effective in degrading BRD4 in all 4 cell lines without regard to the $\alpha_v\beta_3$ integrin status, but SMDC2 and SMDC3 only degrade BRD4 in $\alpha_v\beta_3$ integrin-positive cell lines (HeLa, U87MG, and SK-OV-3). Meanwhile, their proteolysis activity to BRD4 could be inhibited by pretreatment of cells with free cRGD ligand (5 μM), indicating the target selectivity of these SMDCs. This result is in agreement with the observation that the integrin receptor antagonist GLPG0187 can block the SMDCs' cytotoxicity to 22Rv1 cells (Figure S4). To differentiate the potency of the three degraders, we titrated the U87MG cells with serial concentrations of degraders from 0.01 to 1000 nM (Figure 4B). The results show that all three drugs can dose-dependently induce BRD4 degradation with a D_{max} value over 95%. GNE-987 is the most potent degrader, followed by SMDC2 and SMDC3, with DC$_{50}$ values of 0.015, 0.15, and 1.16 nM, respectively. Despite the least potency, SMDC3 remains a potent degrader because near-complete depletion of POI can be achieved at concentrations as low as 3 nM.

In vivo, we observed a high and sustained accumulation of SMDC3 in U87MG tumors, indicating a strong targeting capability (Figures 5A and S5). More importantly, the strong fluorescence signal from SMDC3 persisted in the U87MG tumors for at least 72 h, whereas SMDC2 quickly decayed away in tumors. This observation is consistent with the ex vivo imaging of the dissected tissues (Figure 5B) and the quantitative analysis of drug deposition in tumors (Figure 5C). The increasing deposition of SMDC3 in the tumors is likely attributed to the protraction effect of CBB. As an albumin binder, CBB can hijack the albumin in the bloodstream and prolong the circulation half-life of SMDC it conjugates. The same mode of action has been seen with semaglutide, in which a small-molecule protractor C18 diacid is coupled with GLP1 peptide and increases the circulatory half-life.[36] As depicted in Figure 5D, PK analysis reveals that SMDC3 displays a prolonged PK in mice and its retention in blood can be detected as long as 72 h after intravenous (iv) injection. On the contrary, SMDC2 was eliminated rapidly

https://doi.org/10.1021/acs.jmedchem.5c00862
J. Med. Chem. XXXX, XXX, XXX−XXX

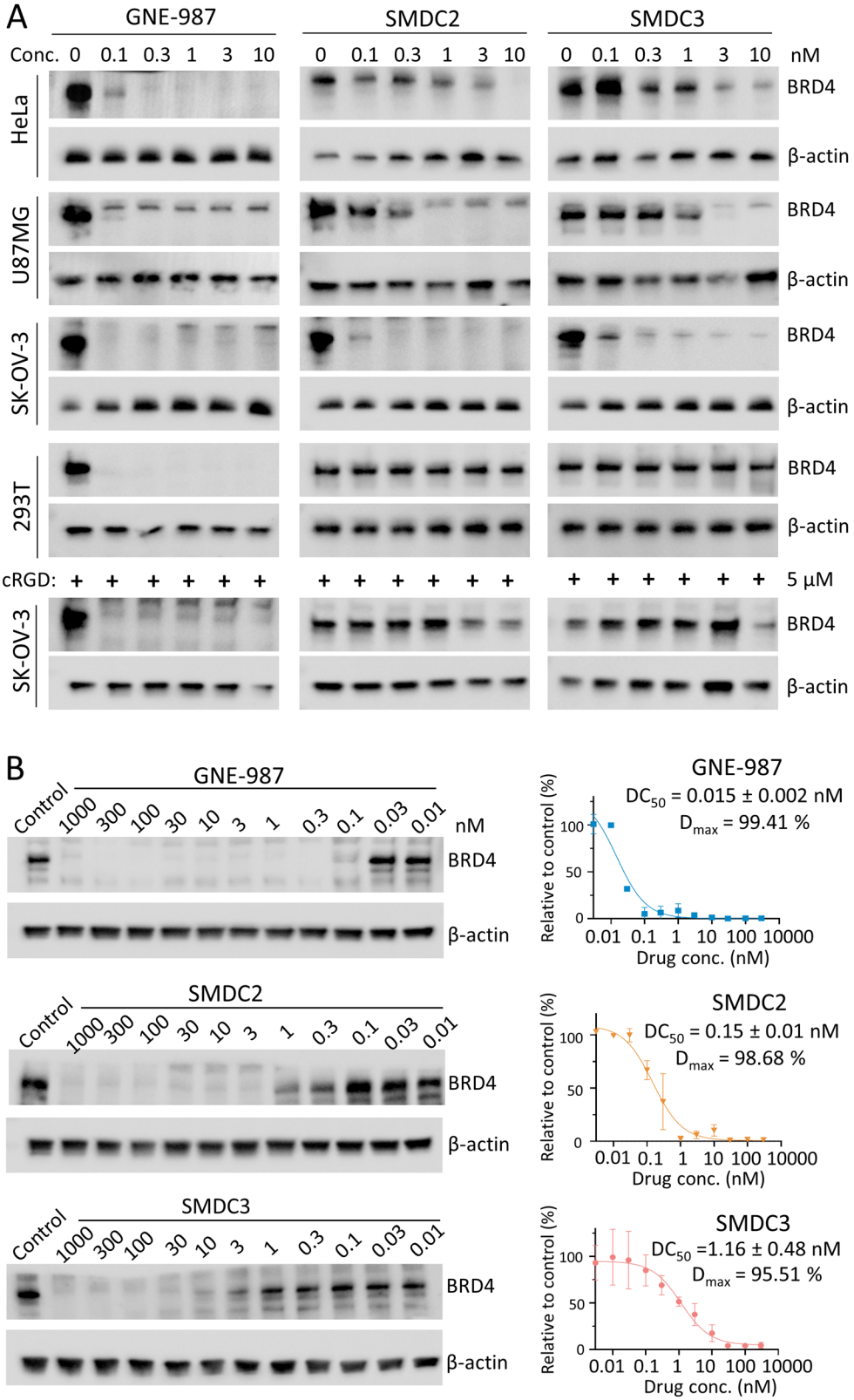

Figure 4. Cell-selective degradation of POIs by SMDCs. (A) Western blot analysis of BRD4 proteolysis in $\alpha_v\beta_3$ integrin-positive cells (HeLa, U87MG, and SK-OV-3), $\alpha_v\beta_3$ integrin-negative cells (293T), and SK-OV-3 cells co-incubated with free cRGD ligand (5 μM). All the cells were treated with serial concentrations of degraders for 12 h before analysis. (B) Analysis of BRD4 degradation in U87MG cells treated with serial dilutions of GNE-987, SMDC2, and SMDC3 (left). The percent remaining of BRD4 protein was plotted for DC_{50} and D_{max} determination (right).

from the circulation, showing a half-life ($T_{1/2}$) as short as 0.7 h. It is remarkable that SMDC3 is only slightly larger than its parent SMDC2 (3.301 vs 2.372 kDa), but albumin recruitment by the CBB can slow down the clearance (CL: 44.82 vs 150.29 mL/h/kg) and maximize the performance in mice (Figure 5E).

https://doi.org/10.1021/acs.jmedchem.5c00862
J. Med. Chem. XXXX, XXX, XXX−XXX

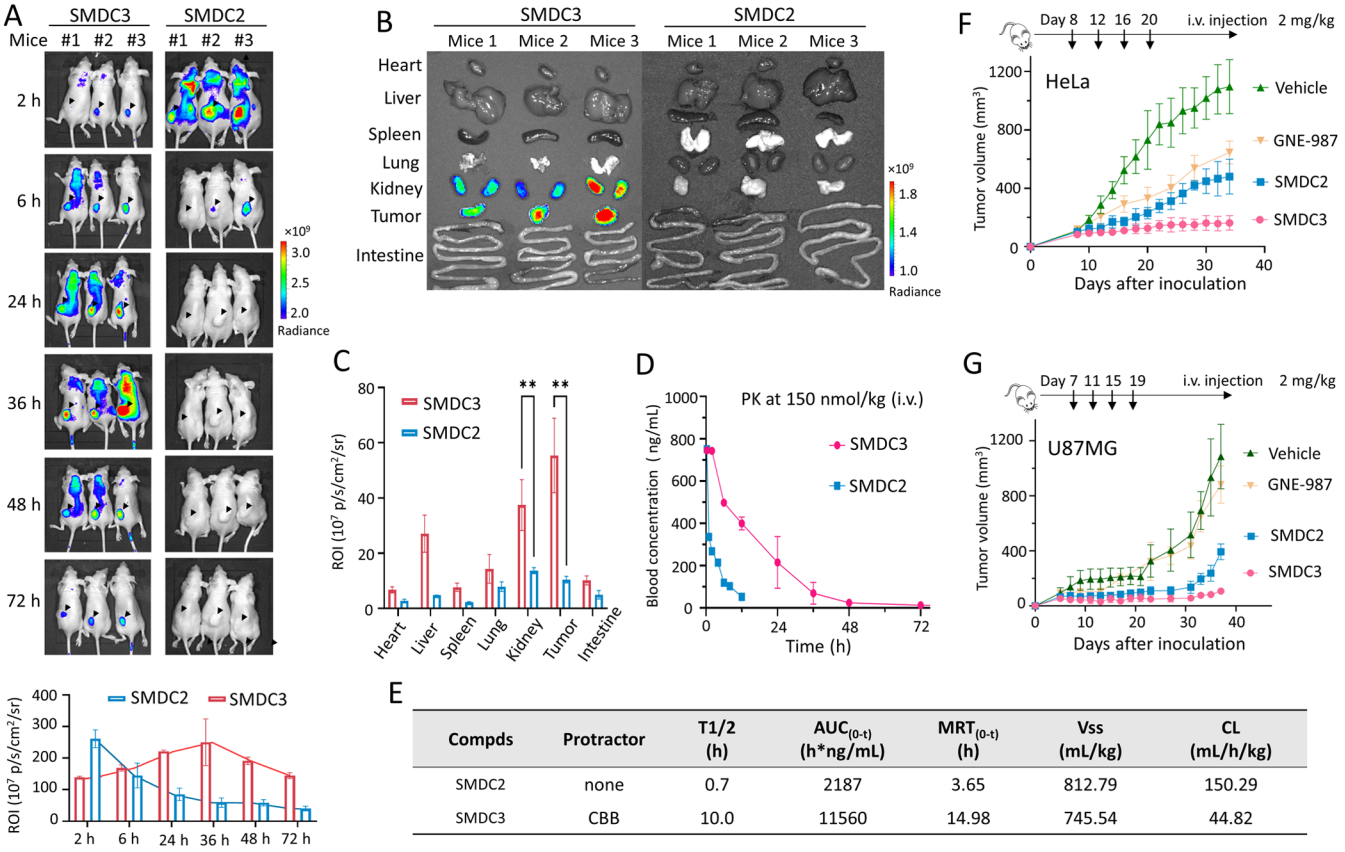

E

Compds	Protractor	T1/2 (h)	$AUC_{(0-t)}$ (h*ng/mL)	$MRT_{(0-t)}$ (h)	Vss (mL/kg)	CL (mL/h/kg)
SMDC2	none	0.7	2187	3.65	812.79	150.29
SMDC3	CBB	10.0	11560	14.98	745.54	44.82

Figure 5. Grafting of CBB protractor to linker (SMDC3) improves the SMDC pharmacokinetics, tumor delivery, and antitumor effect. (A) Biodistribution of sulfo-Cy5.5 labeled SMDC2 and SMDC3 in three mice bearing U87MG tumors. Arrows indicate the tumor sites. The quantitative analysis of tumor signal intensity is listed below (mean ± SD, $n = 3$). (B) Fluorescent images of the dissected organs and tumors at 72 h after injection. (C) Quantitative analysis of average radiant efficiency in organs and tumors of Figure 5B. $^{**}P < 0.01$. (D) The long PK profiles of SMDC3 versus SMDC2 demonstrate a circulation-protracting effect by CBB linkers in mice ($n = 3$). (E) Table showing the key PK parameters of SMDC2 and SMDC3 in BALB/c mice. (F) Tumor growth curves in mice ($n = 5$) treated by GNE-987 (2 mg/kg), SMDC2 (2 mg/kg), and SMDC3 (2 mg/kg) via the intravenous (iv) route. The phosphate-buffered saline (PBS) is used as vehicle control. (G) Growth curves of U87MG xenograft ($n = 5$) after treatment by PBS vehicle, GNE-987 (2 mg/kg), SMDC2 (2 mg/kg), and SMDC3 (2 mg/kg).

We then proceeded to evaluate the therapeutic efficacy of all degraders in mice bearing HeLa (Figure 5E) and U87MG xenografts (Figure 5F). The profound inhibition of tumor growth was observed in animals treated with both SMDCs. However, SMDC3, despite being less potent in vitro, is more effective than SMDC2 in the antitumor experiments. The impressive efficacy of SMDC3 could be ascribed to the long half-life and good serum stability, which benefits from the protractor-bearing carbamate linker. Taken together, these results demonstrate that SMDC3 can produce sustained and tumor-selective bioactivity in vivo.

Cathepsin-Cleavable GGFG Linker Augments the Stability and Therapeutic Efficacy In Vivo. The prolonged half-life of SMDC in circulation pushed us back to reoptimize the linker chemistry. The disulfide-based carbamate linker demonstrated a good serum stability, but a premature leakage of GNE-987 (~23%) was detected after 24 h incubation in mouse serum (Figure 3B). This premature leakage appears to start from the nonspecific cleavage of the disulfide bond by the thiol−disulfide exchange reaction in serum.[37] To design a stable linker, we replaced the disulfide linkage with a GGFG tetrapeptide (Figure 6A). GGFG is a cathepsin-sensitive linker used in the FDA-approved ADC DS-8201a.[38] It is well known for its aqueous solubility and extreme stability in serum, which fits the SMDC requirement. The new SMDC, referred to as SMDC4, is quite stable in 90% mouse serum, without premature release even after 24 h (Figures 6B and S6). The SMDC4 was then applied to the 22Rv1 cell for the POI degradation test. The kinetics experiments reveal that SMDC4 induces fast degradation of BRD4 protein at a concentration as low as 0.3 nM (Figure 6C). Its degradation rate is slightly slower than SMDC3. It is noticed that its DC_{50} and IC_{50} values are higher than SMDC3, which might be ascribed to the necessity of a cathepsin cleavage process for PROTAC release (Figure 6D,E). When a pan-cathepsin inhibitor E64D was co-incubated with 22Rv1 cells, SMDC4 lost its ability to degrade BRD4, indicating the cathepsin responsiveness of SMDC4 (Figure 6C).

The therapeutic efficacy of SMDC4 was evaluated in mice bearing 22Rv1 tumors and compared to SMDC3. A single-dose regimen of SMDC4 was scheduled for parallel comparisons. As shown in Figure 7A, SMDC4 is more profound to retard tumor growth than SMDC3, especially when administered via iv route (Figure 7B). The dose-titration experiment reveals that SMDC4 is effective at all tested doses (from 0.5 to 6 mg/kg). A single dose of 6 mg/kg can arrest the tumor growth in the entire course of treatment, and regrowth was observed 25 days after discontinuation of injection (Figure 7C). To further explore the antitumor potential, the advanced 22Rv1 tumors (tumor burden ~500 mm^3) were established

https://doi.org/10.1021/acs.jmedchem.5c00862
J. Med. Chem. XXXX, XXX, XXX−XXX

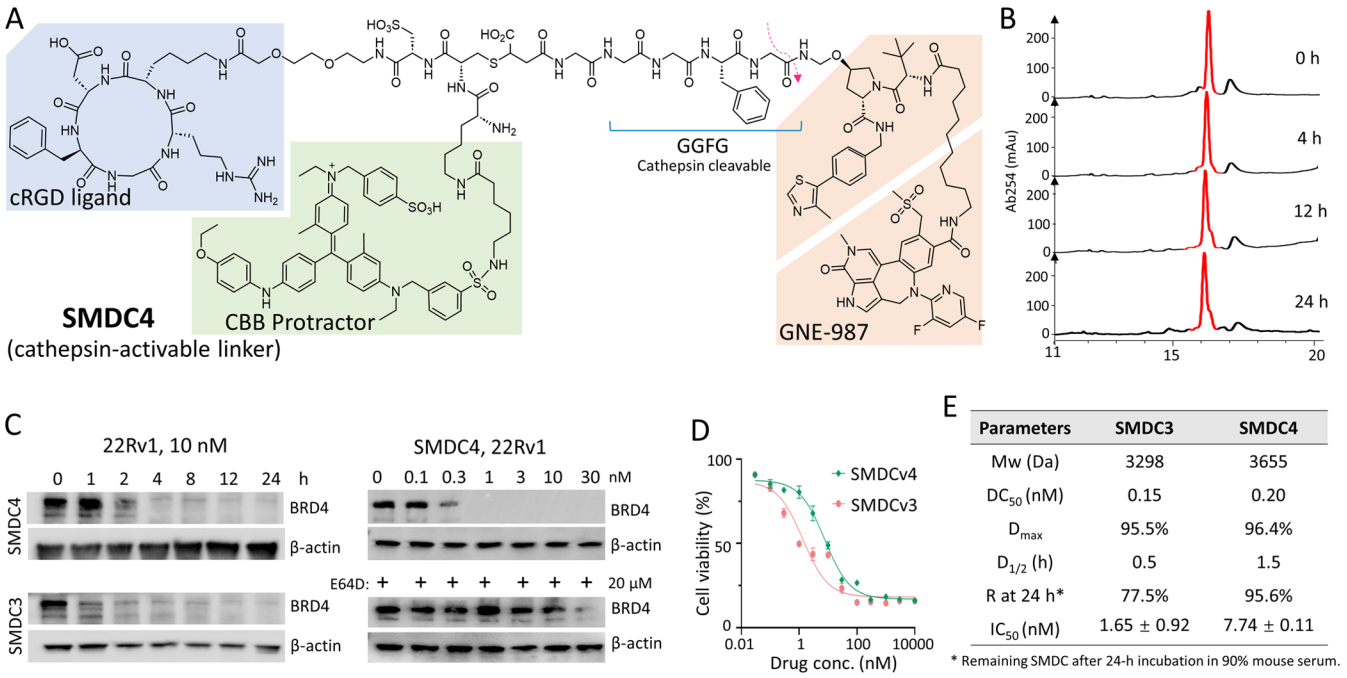

Figure 6. SMDC4 containing a cathepsin-sensitive GGFG linker is better than SMDC3 in aspects of linker stability and in vivo efficacy. (A) Chemical structure of SMDC4. Drug release is triggered by cathepsin-mediated cleavage of the GGFG linker. The dashed red arrow indicates the cleavage position. (B) HPLC evaluation of SMDC4 stability in 90% mouse serum at 37 °C. (C) Immunoblotting to evaluate the degradation kinetics, concentration dependency, and cathepsin sensitivity of SMDC4 in 22Rv1 cells. E64D is a pan-cathepsin inhibitor. (D) Viability profiles of 22Rv1 cells after treatment by SMDC3 and SMDC4 for 72 h. (E) Table summarizing the key parameters of the two SMDC degraders.

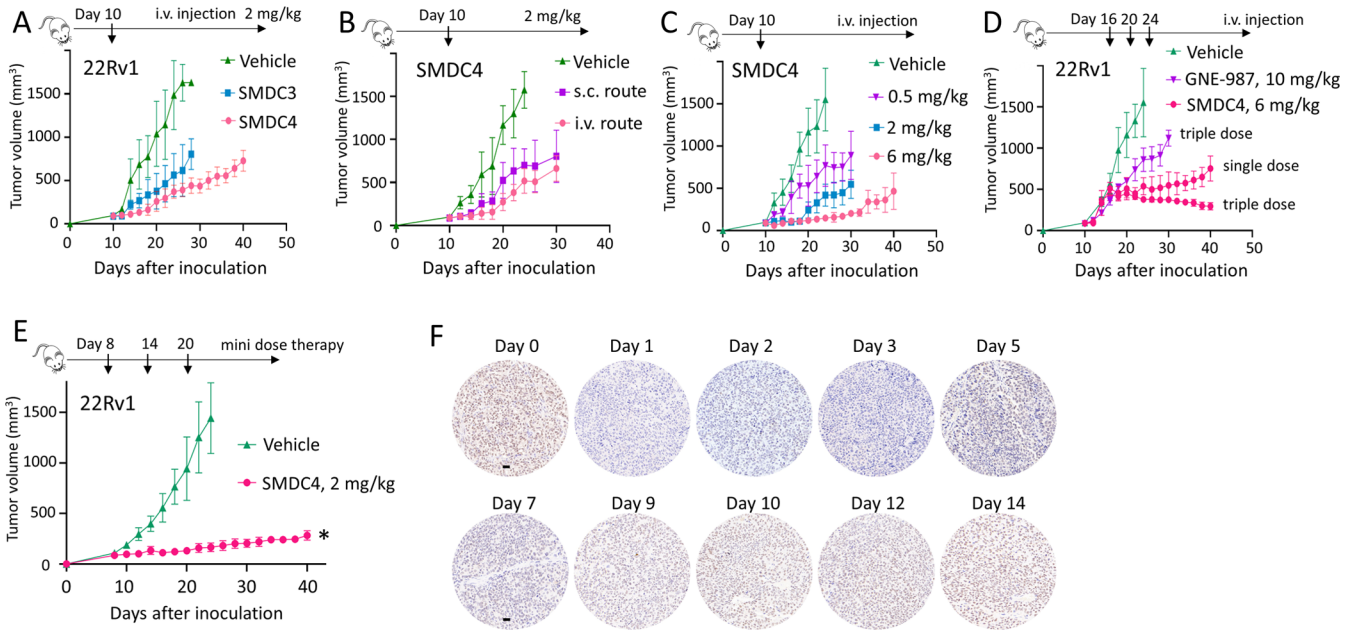

Figure 7. SMDC4 demonstrates a profound antitumor effect at a much reduced PROTAC dose. Tumor volume data are presented as mean ± SD (n = 5). (A) Growth curves of 22Rv1 xenografts after treatment by a single dose (iv, 2 mg/kg) of SMDC3 or SMDC4. (B) Comparison of administration routes to the antitumor effect. 22Rv1 xenograft mice were administered at 2 mg/kg via subcutaneous (sc) or iv route separately. (C) Dose-escalation studies showing a dose-dependent antitumor efficacy of SMDC4 in 22Rv1 xenograft models. (D) Tumor shrinkage in mice bearing the advanced 22Rv1 tumors (500 mm^3). Single-dose or triple-dose SMDC4 (6 mg/kg per dose) is compared to GNE-987 (10 mg/kg) and PBS vehicle. *P < 0.05. (E) Multiple low-dose therapy by SMDC4 in 22Rv1 xenograft models (2 mg/kg). (F) Immunochemical staining to evaluate the degradation duration of BRD4 protein in 22Rv1 tumors receiving a single-dose treatment of SMDC4 (iv, 6 mg/kg). Scale bar, 50 μm.

and challenged by single or triple doses of SMDC4 (6 mg/kg per dose). As shown in Figure 7D, a single injection of SMDC4 led to tumor stabilization for up to 20 days, and triple doses can shrink the tumor size to less than 200 mm^3 in 3 weeks. Eventually, we found that triple injections of SMDC4 at low doses (2 mg/kg) can potentiate the antitumor activity, causing more durable and complete regression than that induced by a single injection (6 mg/kg) (Figure 7E). To assess

https://doi.org/10.1021/acs.jmedchem.5c00862
J. Med. Chem. XXXX, XXX, XXX−XXX

A

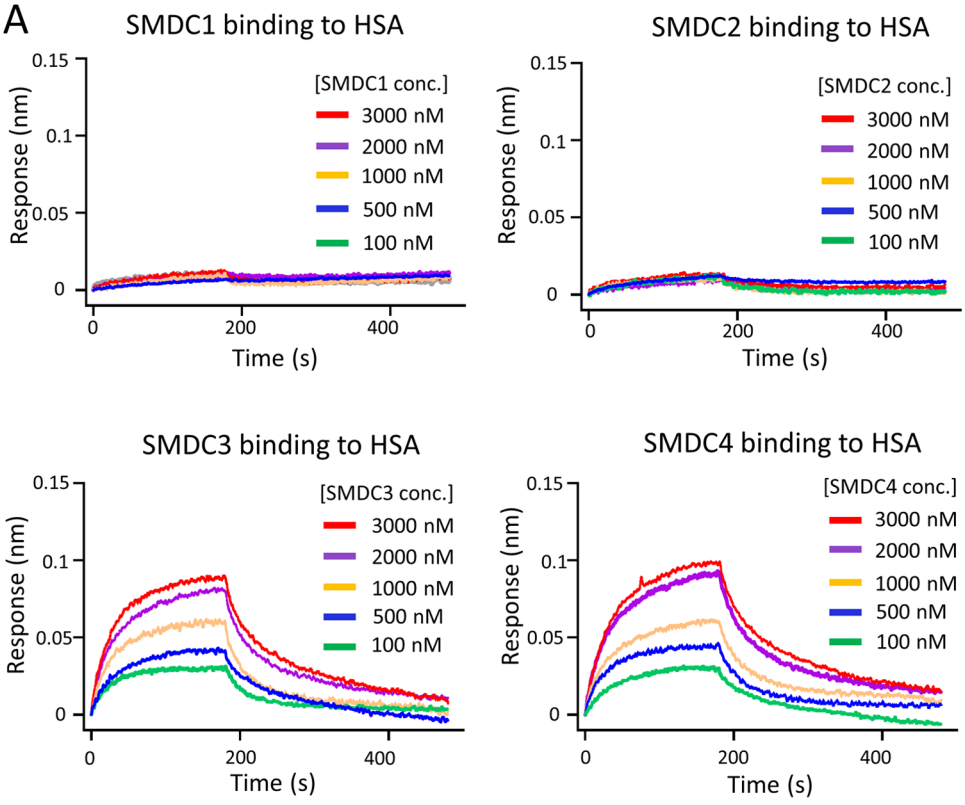

B

Compds	K_{on} (1/Ms)	K_{off} (1/s)	K_D (μM)*
SMDC1	ND	ND	ND
SMDC2	ND	ND	ND
SMDC3	$(8.81 \pm 0.23) \times 10^3$	$(1.51 \pm 0.17) \times 10^{-2}$	1.71 ± 0.15
SMDC4	$(8.16 \pm 0.18) \times 10^3$	$(1.33 \pm 0.20) \times 10^{-2}$	1.62 ± 0.21

* Kinetic K_D values are defined by $K_D = K_{off}/K_{on}$. Some values are not detectable (ND) because the data was not interpretable using standard Langmuir binding kinetics.

Figure 8. Affinity assessment by BLI assays to HSA. (A) BLI sensorgrams of the binding to HSA in response to SMDC concentrations (conc.). (B) Table summarizing the K_{on}, K_{off}, and K_D values (n = 3).

the duration of BRD4 degradation in vivo, mice bearing 22Rv1 tumors were administered with a single dose of SMDC4 (iv, 6 mg/kg), and the treated tumors were dissected at indicated time points for immunohistochemistry (IHC) study. Image analysis of tumor sections reveals that BRD4 immunoreactivity (brown deposits) dramatically reduces in the first 7 days after treatment, but gradually returns to normal at day 14 (Figure 7F). The data demonstrate that SMDC4 is a potent and long-acting degrader in vivo.

The protractor moiety and linker chemistry are keys to achieve the prolonged exposure of GNE-987 and overcome in vivo barriers. We explored the mechanism of CBB as a protractor to prolong the blood retention times of SMDCs. The plausibility stems from the fact that albumin is the most abundant protein in plasma (35 mg/mL) and that CBB can hijack albumin to improve the PKs by binding with it. As shown in Figure 8, we immobilized the human serum albumin (HSA) on the biosensors of Octet biolayer interferometry (BLI) and profiled the dissociation constant (K_D) values of SMDCs to HSA. The steadily increasing BLI response was observed in the HSA-binding assays along with the increment of SMDC3 or SMDC4 concentration, but not that of SMDC1 and SMDC2 (Figure 8A). Langmuir analysis of the binding affinity and kinetics reveals that SMDC3 and SMDC4 display similar affinity to HSA (K_D: 1.71 vs 1.62 μM), whereas SMDC1 and SMDC2 show no binding ability to the immobilized HSA because of the absence of CBB protractor in their structures. It is noted that SMDCs have a fast dissociation rate (K_{off}) from HSA, which enables their traffic from the albumin carriers to the targeted tumor receptors.

The same concept of protraction has been widely used by hydrophobic small-molecule drugs such as paclitaxel to enhance circulatory half-life and bioavailability in vivo.[39] The most elegant example is Semaglutide, which conjugates the

https://doi.org/10.1021/acs.jmedchem.5c00862
J. Med. Chem. XXXX, XXX, XXX−XXX

bioactive peptide GLP1 with an albumin-binding protractor C18 diacid for long-term action. The protractor moiety is the key feature to secure the dose regimen of once-weekly administration, leading to the historic success of semaglutide.[40] In our previous study, we demonstrated that CBB has a high binding affinity to HSA, and can act as a peptide protractor to prolong the therapeutic effect of GLP-1 as good as C18 diacid.[41] In this study, we expanded its application to SMDCs. It is worth mentioning that the binding of CBB to HSA and its protraction effect on SMDCs might be affected by drug−drug interactions or diseased states of patients.[42] Some commonly used drugs such as Warfarin, Bucolome, and Ibuprofen may compete the albumin binding sites of CBB and result in marked changes of the free SMDC concentration in the blood, thus affecting the pharmacokinetic properties.[43] Altered albumin concentration by abnormal physiology, for example, the impairment of liver and kidney function, may also have a serious impact on the protraction effect of CBB. Further studies are encouraged in this regard to exploit its clinical significance for therapeutic purposes.

CONCLUSIONS

Small-molecule ligand-guided PROTAC degraders, termed SMDCs in this study, provide a means to selectively degrade POIs in cancer cells. Compared to DACs, these SMDC degraders offer numerous advantages, such as simple structure, low manufacturing cost, deep penetration, and good immune tolerance. In an effort to obtain a cancer-selective degrader (based on GNE-987), we synthesized the cRGD-based SMDC of the first version (SMDC1) via the thiol-sensitive carbonate linker. The SMDC1 was synthesized through a two-step coupling method. However, its carbonate linker is well known for its feasibility to attack by endogenous esterase. It has been frequently used as the key linkage of prodrugs, for example, Adefovir dipivoxil, Tenofovir disoproxil, and Baloxavir marboxil, in which it helps enhance the oral bioavailability but hydrolyze to the parent drug in the bloodstream.[44] In our study, the carbonate linker was utilized in version 1 because of its ease in synthesis and also several DAC examples of such linkers published in the peer-reviewed literature.[5,12] However, its poor stability in mouse serum prompted us to investigate another carbamate-based disulfide linker. The linker of the second version is much more stable than the carbonate linkage. More strikingly, its stability in mouse serum is further boosted after the protractor CBB molecule is grafted with linkers. The linker of SMDC3 (with a CBB grafted) is stable over 24 h in the mouse serum at 37 °C, enabling the antitumor therapeutic evaluation in mice. The SMDC4, bearing a cathepsin-sensitive GGFG linker, presents as the most stable SMDC format in mouse serum, nearly with no premature leakage. Its advantages in structure are also reflected by the superior therapeutic efficacy in vivo. It is worth noting that GGFG is conjugated to SMDC4 via a maleimide−thiol reaction, which was later hydrolyzed into a more stable ring-opening form by alkaline treatment. This ring-opened maleimide−thiol adduct precludes the possibility of the retro-Michael reaction,[45] minimizes the drug loss during long-term circulation in the blood, and at the same time features enhanced hydrophilicity owing to the nascent carboxylic group.

In summary, we have developed a target degrader to achieve long-term degradation of POI and robust tumor suppression in mice by optimizing the linker chemistry. The SMDC degrader exhibits a long-time residence in blood circulation and shows antitumor activity in vivo. We believe that the SMDC, as a new therapeutic modality that shows a very unique structural profile, may be possible to expand the application of the PROTAC degrader beyond the classic DACs.

EXPERIMENTAL SECTION

General Information for Chemistry. Chemicals and solvents were generally purchased from commercial sources (TCI and Bidepharm) and used directly as received without further purification unless otherwise noted. Flash column chromatography was performed with silica gel (200−300 mesh) purchased from Accela ChemBio. ^{1}H NMR spectra were recorded on a Bruker AMX-400 (400 MHz) in dimethyl sulfoxide (DMSO)-d_6. The chemical shifts are reported in parts per million (ppm) on the δ scale with an internal reference of either tetramethylsilane (δ 0.00 ppm, ^{1}H) or residual DMSO (δ 2.50 ppm, ^{1}H). NMR multiplicities are abbreviated as follows: s = singlet, d = doublet, t = triplet, q = quartet, sept = septet, m = multiplet, and br = broad signal. Coupling constants (J) are reported in hertz. Mass spectroscopy was performed using an LCQ Fleet Ion Trap Mass Spectrometer (Thermo Fisher Scientific) in the Mass Spectrometer Center, School of Pharmaceutical Sciences, Wuhan University. The final compounds were all purified by a C18 reversed-phase preparative HPLC column (Agilent C18 OBD 5 μm, 21 × 100 mm^2) with solvent A (0.1% formic acid (FA) in H_2O) and solvent B (0.1% formic acid in MeCN). The purity of all the final compounds was measured and confirmed to be >95% by HPLC analysis.

Compound **2**. To a solution of (*S*,*R*,*S*)-AHPC (**1**) (200 mg, 0.47 mmol) in DMF (2 mL) were added Fmoc-11-Aun-OH (25 mg, 0.47 mmol), HATU (359 mg, 0.95 mmol), and DIPEA (170 mg, 1.41 mmol). After being stirred at room temperature for 1 h, the organic layer was concentrated under reduced pressure. The crude residue was purified by flash column chromatography with DCM/MeOH (20:1) to obtain compound **2** (200 mg, yield: 52%). ^{1}H NMR (400 MHz, DMSO-d_6) δ 8.98 (s, 1H), 8.60 (t, J = 6.1 Hz, 1H), 7.88 (d, J = 7.5 Hz, 3H), 7.67 (d, J = 7.5 Hz, 2H), 7.39 (q, J = 8.3, 7.9 Hz, 6H), 7.31 (t, J = 7.1 Hz, 3H), 5.15 (d, J = 3.5 Hz, 1H), 4.53 (d, J = 9.3 Hz, 1H), 4.47−4.41 (m, 1H), 4.40 (d, J = 7.7 Hz, 1H), 4.34 (s, 1H), 4.28 (d, J = 6.9 Hz, 2H), 4.23−4.17 (m, 2H), 3.65 (d, J = 4.2 Hz, 2H), 2.94 (q, J = 6.5 Hz, 2H), 2.43 (s, 3H), 2.24 (dd, J = 13.9, 7.0 Hz, 1H), 2.12−2.06 (m, 1H), 2.05−1.98 (m, 1H), 1.93−1.82 (m, 1H), 1.54−1.40 (m, 2H), 1.40−1.31 (m, 2H), 1.22 (s, 12H), 0.92 (s, 9H). ^{13}C NMR (151 MHz, DMSO-d_6) δ 172.09, 156.06, 151.44, 147.71, 143.94, 140.74, 129.63, 128.63, 127.58, 127.42, 127.01, 125.13, 120.11, 68.86, 65.11, 56.26, 54.91, 53.57, 46.78, 41.82, 41.64, 37.96, 35.21, 29.36, 28.99, 28.93, 28.77, 28.74, 28.67, 26.23, 25.45, 18.08, 16.73, 15.94. High-resolution mass spectrometry (HRMS) (ESI): m/z calcd for $C_{48}H_{62}N_5O_6S$ $[M + H]^+$ 836.4421, found 836.4429.

Compound **3**. To a solution of compound **2** (200 mg, 0.24 mmol) dissolved in 1 mL of DMF were added bis(4-nitrophenyl) carbonate (143 mg, 0.47 mmol) and DIPEA (57 mg, 0.47 mmol). After being stirred at room temperature for 2 h, the organic layer was concentrated under reduced pressure. The crude residue was purified by flash column chromatography with DCM/MeOH (40:1) to obtain compound **3** (200 mg, yield: 84%). ^{1}H NMR (600 MHz, chloroform-d) δ 8.69 (s, 1H), 8.26 (d, J = 9.2 Hz, 2H), 8.12 (d, J = 9.2 Hz, 1H), 7.76 (d, J = 7.6 Hz, 2H), 7.58 (d, J = 7.4 Hz, 2H), 7.52 (d, J = 9.2 Hz, 2H), 7.38 (dd, J = 13.9, 6.5 Hz, 4H), 7.35 (d, J = 8.2 Hz, 3H), 7.30 (t, J = 7.4 Hz, 2H), 6.90 (d, J = 9.2 Hz, 1H), 6.02 (d, J = 9.0 Hz, 1H), 4.80 (t, J = 7.9 Hz, 2H), 4.54 (s, 1H), 4.38 (d, J = 6.9 Hz, 2H), 4.36−4.30 (m, 1H), 3.80−3.76 (m, 1H), 3.74−3.68 (m, 2H), 3.17 (q, J = 7.4 Hz, 4H), 2.97 (s, 1H), 2.51 (s, 3H), 2.41−2.34 (m, 1H), 2.25 (d, J = 9.1 Hz, 1H), 2.17 (t, J = 7.7 Hz, 2H), 1.42 (s, 4H), 1.19 (s, 10H), 0.91 (s, 9H). ^{13}C NMR (151 MHz, chloroform-d) δ 150.62, 145.69, 144.13, 141.44, 129.74, 128.40, 127.80, 127.16, 126.29, 125.35, 125.17, 122.40, 120.10, 115.80, 58.28, 57.34, 55.86, 53.81, 47.42, 43.80, 43.60, 41.21, 36.52, 34.92, 26.81, 26.47, 25.69, 16.12, 12.65. MS (ESI): m/z calcd for $C_{55}H_{65}N_6O_{10}S$ $[M + H]^+$ 1001.45, found 1001.45.

https://doi.org/10.1021/acs.jmedchem.5c00862
J. Med. Chem. XXXX, XXX, XXX−XXX

Compound 5. The key intermediate 2-(2-pyridinyldithio)-1-propanol, namely, compound **4**, was synthesized according to the previously reported procedure.[46] To a solution of compound **3** (200 mg, 0.20 mmol) dissolved in 4 mL of DCM were added compound **4** (150 mg, 0.75 mmol) and TEA (180 mg, 1.5 mmol), DMAP (12 mg, 0.10 mmol). After being stirred at room temperature for 3 h, the organic layer was concentrated under reduced pressure. The crude residue was purified by flash column chromatography with DCM/MeOH (20:1) to obtain compound **6** (200 mg, yield: 94%). ^{1}H NMR (600 MHz, DMSO-d_6) δ 8.99 (s, 1H), 8.62 (t, J = 6.0 Hz, 1H), 8.43 (d, J = 4.7 Hz, 1H), 7.88 (d, J = 7.3 Hz, 3H), 7.81 (t, J = 7.7 Hz, 1H), 7.76 (d, J = 8.1 Hz, 1H), 7.68 (d, J = 7.5 Hz, 2H), 7.43−7.38 (m, 6H), 7.31 (t, J = 7.4 Hz, 2H), 7.26−7.21 (m, 2H), 5.17 (s, 1H), 4.45 (t, J = 8.2 Hz, 2H), 4.39 (d, J = 8.9 Hz, 1H), 4.28 (d, J = 7.0 Hz, 2H), 4.23 (s, 1H), 4.22−4.18 (m, 2H), 4.13 (d, J = 14.0 Hz, 2H), 3.82 (d, J = 15.4 Hz, 1H), 3.40−3.34 (m, 1H), 2.95 (q, J = 6.6 Hz, 2H), 2.44 (s, 3H), 2.31 (d, J = 10.4 Hz, 1H), 2.23 (d, J = 13.3 Hz, 1H), 2.15−2.06 (m, 2H), 1.44 (d, J = 31.8 Hz, 2H), 1.37 (s, 2H), 1.29−1.25 (m, 3H), 1.20 (s, 12H), 0.95 (s, 9H). ^{13}C NMR (151 MHz, DMSO-d_6) δ: 172.51, 169.91, 156.08, 153.57, 151.52, 149.44, 143.95, 140.75, 139.34, 128.69, 127.58, 127.46, 127.02, 125.14, 121.30, 119.38, 77.14, 69.40, 65.13, 58.20, 56.88, 53.39, 46.80, 41.70, 40.21, 34.74, 34.70, 34.59, 29.38, 29.02, 28.96, 28.79, 28.76, 28.68, 26.34, 26.25, 25.43. MS (ESI): m/z calcd for $C_{57}H_{71}N_6O_8S_3$ $[M + H]^+$ 1063.45, found 1063.75.

Linker-GNE987 (7). To a solution of compound **5** (200 mg, 0.19 mmol) in DMF (1 mL) was added TEA (0.2 mL). After being stirred at room temperature for 4 h, the resulting mixture was concentrated to afford compound **6** as a crude yellow oil (120 mg). To a solution of compound **6** (20 mg, 0.02 mmol) in DMF (2 mL) were added PROTAC BRD4 ligand-1 (12 mg, 0.02 mmol), HATU (15 mg, 0.04 mmol), and DIPEA (5 mg, 0.04 mmol). After being stirred at room temperature for 1 h, the organic layer was concentrated under reduced pressure. The crude residue was purified by flash column chromatography with DCM/MeOH (20:1) to obtain Linker-GNE987 (**7**) (15 mg, yield: 48%). ^{1}H NMR (400 MHz, DMSO-d_6) δ 11.95 (s, 1H), 8.99 (s, 1H), 8.64 (t, J = 6.0 Hz, 1H), 8.47−8.39 (m, 2H), 8.07 (s, 1H), 7.92 (s, 2H), 7.80 (d, J = 7.2 Hz, 1H), 7.77 (d, J = 6.6 Hz, 2H), 7.65−7.60 (m, 1H), 7.40 (d, J = 3.7 Hz, 3H), 7.27 (d, J = 3.4 Hz, 2H), 7.26−7.21 (m, 1H), 6.59 (s, 1H), 5.99 (s, 1H), 5.17 (s, 1H), 4.47−4.34 (m, 4H), 4.23 (d, J = 33.2 Hz, 3H), 4.19−4.08 (m, 3H), 3.82 (d, J = 15.4 Hz, 2H), 3.62 (s, 3H), 3.13 (s, 2H), 2.91 (s, 3H), 2.44 (s, 3H), 2.30 (s, 1H), 2.21 (s, 1H), 2.12 (d, J = 18.6 Hz, 2H), 1.45 (d, J = 2.8 Hz, 4H), 1.27 (d, J = 6.9 Hz, 3H), 1.21 (d, J = 17.1 Hz, 12H), 0.94 (s, 9H). MS (ESI): m/z calcd for $C_{65}H_{77}F_2N_{10}O_{10}S_4$ $[M + H]^+$ 1323.47, found 1323.53. HPLC (purity): 98.60% (λ = 254 nm, t_R = 17.231 min).

Compound 8. To a solution of compound **4** (100 mg, 0.50 mmol) dissolved in 1 mL of DMF were added bis(4-nitrophenyl) carbonate (304 mg, 1.00 mmol) and DIPEA (129 mg, 1.00 mmol). After being stirred at room temperature for 2 h, the organic layer was concentrated under reduced pressure. The crude residue was purified by flash column chromatography with DCM/MeOH (40:1) to obtain compound **8** (100 mg, yield: 55%). ^{1}H NMR (400 MHz, chloroform-d) δ 8.47 (d, J = 3.3 Hz, 1H), 8.26 (s, 2H), 7.75 (d, J = 8.1 Hz, 1H), 7.67 (td, J = 7.7, 1.8 Hz, 1H), 7.37 (d, J = 9.2 Hz, 2H), 7.16−7.11 (m, 1H), 4.44 (dd, J = 11.1, 5.9 Hz, 1H), 4.31 (dd, J = 11.1, 6.7 Hz, 1H), 3.34 (q, J = 6.8 Hz, 1H), 1.42 (d, J = 7.0 Hz, 3H). ^{13}C NMR (151 MHz, DMSO-d_6) δ: 159.06, 155.19, 151.75, 149.55, 145.23, 125.45, 122.58, 121.44, 119.54, 70.58, 43.92, 16.53. MS (ESI): m/z calcd for $C_{15}H_{15}N_2O_5S_2$ $[M + H]^+$ 367.04, found 367.29.

Compound 9. To a solution of compound **8** (100 mg, 0.27 mmol) in pyridine (2 mL) was added NH_3 in 1,4-dioxane (0.4 M, 2 mL). After being stirred at room temperature for 3 h, the organic layer was concentrated under reduced pressure. The crude residue was purified by flash column chromatography with petroleum ether/ethyl acetate (PE/EA) (1:1) to obtain compound **9** (50 mg, yield: 75%). ^{1}H NMR (400 MHz, chloroform-d) δ 8.48 (d, J = 5.6 Hz, 1H), 7.75 (d, J = 8.1 Hz, 1H), 7.72−7.63 (m, 1H), 7.16−7.07 (m, 1H), 4.72 (s, 2H), 4.21−4.10 (m, 2H), 3.24 (q, J = 6.4 Hz, 1H), 1.34 (d, J = 7.0 Hz, 3H). ^{13}C NMR (151 MHz, DMSO-d_6) δ: 159.50, 156.32, 149.39, 137.80, 121.18, 119.17, 65.37, 44.94, 16.76. MS (ESI): m/z calcd for $C_9H_{13}N_2O_2S_2$ $[M + H]^+$ 245.04, found 245.41.

Compound 10. To a stirred solution of compound **9** (50 mg, 0.20 mmol) in acetic acid (0.59 mL) were added paraformaldehyde (0.01 g, 0.47 mmol) and acetic anhydride (2.00 mL). The mixture was heated at 75 °C for 1 h. After completion of the reaction, the reaction was quenched with H_2O (20 mL) and extracted with DCM (20 mL × 2). The combined organic layer was washed with H_2O (20 mL). The crude residue was purified by flash column chromatography with PE/EA (1:1) to obtain compound **10** (50 mg, yield: 77%). ^{1}H NMR (400 MHz, chloroform-d) δ 8.47 (d, J = 4.4 Hz, 1H), 7.77−7.60 (m, 2H), 7.16−7.07 (m, 1H), 5.17 (d, J = 7.5 Hz, 2H), 4.25−4.13 (m, 2H), 3.25 (dq, J = 13.3, 6.6 Hz, 1H), 2.07 (s, 3H), 1.33 (d, J = 7.0 Hz, 3H). ^{13}C NMR (151 MHz, DMSO-d_6) δ: 170.09, 159.33, 155.73, 149.43, 137.79, 121.23, 119.22, 66.61, 66.25, 44.60, 20.78, 16.67. HRMS (ESI): m/z calcd for $C_{12}H_{17}N_2O_4S_2$ $[M + H]^+$ 317.0630, found 317.0630.

Compound 11. To a solution of compound **10** (50 mg, 0.15 mmol) dissolved in 1 mL of DCM were added compound **2** (100 mg, 0.12 mmol) and PPTS (60 mg, 0.24 mmol). After being stirred at 40 °C for 24 h, the organic layer was concentrated under reduced pressure. The crude residue was purified by flash column chromatography with DCM/MeOH (20:1) to obtain compound **11** (50 mg, yield: 38%). ^{1}H NMR (600 MHz, DMSO-d_6) δ 8.98 (s, 1H), 8.56 (t, J = 6.0 Hz, 1H), 8.43 (d, J = 4.7 Hz, 1H), 8.19 (t, J = 6.6 Hz, 1H), 7.88 (d, J = 7.4 Hz, 3H), 7.80 (d, J = 3.9 Hz, 2H), 7.68 (d, J = 7.4 Hz, 2H), 7.40 (q, J = 8.1 Hz, 6H), 7.32 (t, J = 7.4 Hz, 2H), 7.23 (dq, J = 8.6, 4.9, 4.3 Hz, 2H), 4.56−4.52 (m, 1H), 4.51 (s, 2H), 4.41 (d, J = 9.9 Hz, 2H), 4.29 (d, J = 6.9 Hz, 3H), 4.26−4.18 (m, 2H), 4.13−4.03 (m, 2H), 3.93 (d, J = 11.1 Hz, 1H), 3.67 (d, J = 13.5 Hz, 1H), 3.32−3.27 (m, 1H), 3.14 (s, 1H), 2.95 (d, J = 12.9 Hz, 2H), 2.44 (s, 3H), 2.29−2.21 (m, 1H), 2.15 (d, J = 21.7 Hz, 2H), 1.97 (s, 1H), 1.45 (s, 2H), 1.37 (s, 2H), 1.26 (d, J = 6.9 Hz, 3H), 1.22 (s, 12H), 0.94 (s, 9H). ^{13}C NMR (151 MHz, DMSO-d_6) δ: 171.67, 156.08, 151.46, 149.39, 143.94, 140.74, 139.42, 137.77, 128.66, 127.59, 127.44, 125.14, 121.20, 74.20, 66.00, 65.13, 58.46, 56.54, 54.92, 53.60, 46.79, 41.65, 35.24, 34.81, 29.37, 29.00, 28.95, 28.78, 28.75, 28.67, 26.38, 26.24, 25.47, 18.09, 16.70, 15.95. HRMS (ESI): m/z calcd for $C_{58}H_{74}N_7O_8S_3$ $[M + H]^+$ 1092.4761, found 1092.4773; for $[M+2H]^{2+}$ 546.7414, found 546.7435.

Linker-GNE987 (13). To a solution of compound **11** (50 mg, 0.04 mmol) in DMF (2 mL) was added TEA (0.4 mL). After being stirred at room temperature for 4 h, the resulting mixture was concentrated to afford compound **12** as a crude yellow oil (30 mg). The product was directly used for the next step. To a solution of compound **12** (30 mg, 0.03 mmol) in DMF (2 mL) were added PROTAC BRD4 ligand-1 (12 mg, 0.02 mmol), HATU (15 mg, 0.04 mmol), and DIPEA (5 mg, 0.04 mmol). After being stirred at room temperature for 1.5 h, the organic layer was concentrated under reduced pressure. The crude residue was purified by flash column chromatography with DCM/MeOH (10:1) to obtain Linker-GNE987 (**13**) (10 mg, yield: 31%). HRMS (ESI): m/z calcd for $C_{66}H_{80}F_2N_{11}O_{10}S_4$ $[M + H]^+$ 1352.4941, found 1352.4959; for $[M + 2H]^{2+}$ 676.7504, found 676.7526. HPLC (purity): 99.11% (λ = 254 nm, t_R = 17.265 min).

Compound 19. Compound **15** was synthesized on 2-chlorobenzoyl chloride resin (2-Cl Trt resin) following the standard solid-phase peptide synthesis protocol. Compound **17** was cleaved from the resin with a mixture of acetic acid (1 mL), TFE (2 mL), and DCM (7 mL) at room temperature for 2 h, the filtrate was combined and the solvent was removed in vacuo. The crude product was loaded onto a silica gel column and purified by chromatography (DCM/MeOH/AcOH = 50:1:0.1) to afford compound **17** as a white solid (500 mg, 45%). To a solution of compound **17** (500 mg, 0.45 mmol) in DCM (4 mL) were added HOSu (104 mg, 0.90 mmol) and EDCI (154 mg, 1.00 mmol). After being stirred at room temperature for 4 h, the resulting mixture was purified by preparative HPLC (5−100% acetonitrile/0.1% FA in H_2O). The product-containing fractions were concentrated to remove the organic solvent under reduced pressure and then dried by lyophilization to afford compound **19** as a light

https://doi.org/10.1021/acs.jmedchem.5c00862
J. Med. Chem. XXXX, XXX, XXX−XXX

yellow solid (400 mg, 76%). MS (ESI): m/z calcd for $C_{61}H_{69}N_6O_{16}S_2$ $[M - H]^-$ 1205.42, found 1205.43.

*Compound **20***. Compound **16** was then derived by introducing Ahx-CBB to compound **15**. Compound **18** was cleaved from the resin with a mixture of acetic acid (1 mL), TFE (2 mL), and DCM (7 mL) at room temperature for 2 h, the filtrate was combined, and the solvent was removed in vacuo. The crude product was loaded onto a silica gel column and purified by chromatography (DCM/MeOH/AcOH = 50:1:0.1) to afford compound **18** as a blue solid (25 mg, 78%). To a solution of compound **18** (25 mg, 0.01 mmol) in DCM (4 mL) were added HOSu (6 mg, 0.05 mmol) and EDCI (9 mg, 0.06 mmol). After being stirred at room temperature for 4 h, the resulting mixture was purified by preparative HPLC (5−100% acetonitrile/0.1% FA in H_2O). The product-containing fractions were concentrated to remove the organic solvent under reduced pressure and then dried by lyophilization to afford compound **20** as a blue solid (20 mg, 76%).

*Compound **21***. To a solution of compound **19** (400 mg, 0.33 mmol) in DMF (2 mL) were added cRGD (200 mg, 0.33 mmol) and DIPEA (85 mg, 0.66 mmol). After being stirred at room temperature for 4 h, the resulting mixture was purified by preparative HPLC (5−100% acetonitrile/0.1% FA in H_2O). The product-containing fractions were concentrated to remove the organic solvent under reduced pressure and then dried by lyophilization to afford compound **21** as a white solid (200 mg, 36%). HRMS (ESI): m/z calcd for $C_{84}H_{105}N_{14}O_{20}S_2$ $[M - H]^-$ 1693.7071, found 1693.7077.

*Compound **22***. To a solution of compound **20** (20 mg, 0.01 mmol) in DMF (2 mL) were added cRGD (12 mg, 0.02 mmol) and DIPEA (4 mg, 0.03 mmol). After being stirred at room temperature for 1 h, the resulting mixture was purified by preparative HPLC (5−100% acetonitrile/0.1% FA in H_2O). The product-containing fractions were concentrated to remove the organic solvent under reduced pressure and then dried by lyophilization to afford compound **22** as a white solid (20 mg, 84%). HRMS (ESI): m/z calcd for $C_{122}H_{155}N_{18}O_{25}S_4$ $[M - H]^-$ 2399.0210, found 2399.0158.

*Compound **23***. To a solution of compound **21** (150 mg, 0.090 mmol) in DCM (1 mL) was added TFA (0.5 mL). After being stirred at room temperature for 2 h, the resulting mixture was purified by preparative HPLC (5−100% acetonitrile/0.1% FA in H_2O). The product-containing fractions were concentrated to remove the organic solvent under reduced pressure and then dried by lyophilization to afford compound **23** as a white solid (100 mg, 84%). HRMS (ESI): m/z calcd for $C_{60}H_{85}N_{14}O_{18}S_2$ $[M + H]^+$ 1353.5608, found 1353.5575.

*Compound **24***. To a solution of compound **23** (100 mg, 0.07 mmol) in DMF (2 mL) was added TEA (0.5 mL). After being stirred at room temperature for 4 h, the resulting mixture was concentrated to afford compound 24 as a crude yellow oil (100 mg). HRMS (ESI): m/z calcd for $C_{45}H_{75}N_{14}O_{16}S_2$ $[M + H]^+$ 1131.4927, found 1131.4926. HPLC (purity): 97.37% (λ = 280 nm, t_R = 7.659 min).

*Compound **25***. To a solution of compound **22** (20 mg, 0.008 mmol) in DCM (1 mL) was added TFA (0.5 mL). After being stirred at room temperature for 2 h, the resulting mixture was purified by preparative HPLC (5−100% acetonitrile/0.1% FA in H_2O). The product-containing fractions were concentrated to remove the organic solvent under reduced pressure and then dried by lyophilization to afford compound **25** as a blue solid (15 mg, 88%). HRMS (ESI): m/z calcd for $C_{98}H_{132}N_{18}O_{23}S_4$ $[M - H]^-$ 2056.8590, found 2056.8548. HPLC (purity): 99.40% (λ = 612 nm, t_R = 15.114 min).

*Compound **SMDC1***. To a solution of Linker-GNE987 (7) (10 mg, 0.008 mmol) in DMF (1 mL) was added compound **24** (10 mg, 0.009 mmol). After being stirred at room temperature for 4 h, the resulting mixture was purified by preparative HPLC (5−100% acetonitrile/0.1% FA in H_2O). The product-containing fractions were concentrated to remove the organic solvent under reduced pressure and then dried by lyophilization to afford SMDC1 as a white solid (5 mg, 28%). HRMS (ESI): m/z calcd for $C_{105}H_{147}F_2N_{23}O_{26}S_5$ $[M + 2H]^{2+}$ 1171.9730, found 1171.9768. HPLC (purity): 99.29% (λ = 254 nm, t_R = 13.239 min).

*Compound **SMDC2***. Following a procedure similar to that for compound **SMDC1**, compound **SMDC2** was obtained as a white solid (6 mg, 25%). HRMS (ESI): m/z calcd for $C_{106}H_{150}F_2N_{24}O_6S_5$ $[M + 2H]^{2+}$ 1186.4863, found 1186.4901. HPLC (purity): 97.19% (λ = 254 nm, t_R = 13.207 min).

*Compound **SMDC3***. Following a procedure similar to that for compound **SMDC1**, compound **SMDC3** was obtained as a blue solid (6 mg, 38%). HRMS (ESI): m/z calcd for $C_{159}H_{209}F_2N_{28}O_{33}S_7$ $[M + 2H]^{2+}$ 1650.1772, found 1650.1760. HPLC (purity): 99.90% (λ = 612 nm, t_R = 16.683 min).

*Compound **SMDC4a***. Following a procedure similar to that for compound **SMDC1**, compound **SMDC4a** was obtained as a blue solid (7 mg, 30%). HRMS (ESI): m/z calcd for $C_{176}H_{225}F_2N_{33}O_{38}S_6$ $[M + 2H]^{2+}$ 1819.7526, found 1819.7587.

*Compound **SMDC4***. Compound **SMDC4a** (7 mg, 0.002 mmol) was dissolved in 0.1 M $NaHCO_3$/DMF (v/v = 1:1). After being stirred at room temperature for 5 h, the resulting mixture was purified by preparative HPLC (5−100% acetonitrile/0.1% FA in H_2O). The product-containing fractions were concentrated to remove the organic solvent under reduced pressure and then dried by lyophilization to afford **SMDC4** as a blue solid (5 mg, 70%). HRMS (ESI): m/z calcd for $C_{176}H_{228}F_2N_{33}O_{39}S_6$ $[M + 2H]^{2+}$ 1828.7580, found 1828.7622; for $[M + 3H]^{3+}$ 1219.5075, found 1219.5130. HPLC (purity): 97.91% (λ = 612 nm, t_R = 16.351 min).

Cell Lines. HeLa, 22RV1, U87MG, SK-OV-3, 293T, and RWPE-1 were purchased from the American Type Culture Collection (ATCC). Upon thawing, all cells were cultured in Roswell Park Memorial Institute 1640 medium (RPMI 1640, Pricella) supplemented with 10% fetal bovine serum (FBS, Pricella) and 1% penicillin−streptomycin (PS, Pricella). All cells were cultured at 37 °C with 5% CO_2 and regularly checked for the absence of mycoplasma.

Stability Test by HPLC. For the serum stability assay, SMDC1, SMDC2, SMDC3, and SMDC4 were mixed with mouse serum at a volume ratio of 1:9 to reach a final drug concentration of 100 μg/mL. The mixture was incubated at 37 °C, and an aliquot (50 μL) was collected at indicated time points. The aliquot was immediately mixed with 150 μL of MeOH to precipitate the proteins. After centrifugation for 5 min at 10 000g, the supernatant was collected and stored at −80 °C for HPLC assay later. HPLC analysis was performed with a Shimadzu LC-40 system (Shimadzu, Japan) equipping a WondaSil C18 Superb 5 μm 4.6 mm × 150 mm column (GL Sciences). The mobile phase consisted of buffer A (water plus 0.1% formic acid) and buffer B (acetonitrile plus 0.1% formic acid) with a flow rate of 1 mL/min and gradient elution for 30 min. The running program is as follows: 95% buffer A and 5 buffer B adjust to 5% buffer A and 95% buffer B as a gradient from 0 to 20 min, maintain 5% buffer A and 95% buffer B from 20 to 24 min, and maintain 95% buffer A and 5% buffer B from 24 to 30 min.

To assess the stability and drug release after DDT treatment, the stock (200 μM) of SMDC1, SMDC2, and SMDC3 in DMSO was diluted to PBS buffer to reach a final concentration of 10 μM (0.5 mL). 5 μL of DTT (5 mM) was added and incubated at 37 °C. At indicated time points (0.1 or 0.5, 1, and 1.5 h), 50 μL of the reaction was sampled and analyzed by RP-HPLC.

Cell Binding Analysis by Flow Cytometry. SMDC2 or SMDC3 (sulfo-Cy5 labeled, Duoflour) was diluted with RPMI 1640 or RPMI 1640 containing 10% FBS to 50 nM and incubated with cancer cells (100 000 cells) for 2 h at room temperature. The cells were washed twice with PBS and analyzed on a BD LSR II flow cytometer (Beckton Dickinson).

Western Blotting Analysis. The cells were inoculated in 6-well plates at a density of 3×10^5 cells per well and incubated for 12 h. Cells were then treated with either DMSO or the compounds for a designated period. After incubation, the culture medium was discarded and the tumor cells were washed with PBS and lysed with IP buffer (Beyotime P0013). The lysate was centrifuged at 13 000 rpm for 10 min at 4 °C. The supernatant was collected, and protein concentration was determined using a BCA Assay Kit (Thermo A55860). Protein samples (20 μg) were loaded onto a 4−20

https://doi.org/10.1021/acs.jmedchem.5c00862
J. Med. Chem. XXXX, XXX, XXX−XXX

or 8% sodium dodecyl sulfate-polyacrylamide gel (SDS-PAGE) and subjected to electrophoresis at 120 V for 2 h. Proteins were then transferred to an immobilized poly(vinylidene difluoride) (PVDF) membrane (Millipore IPVH00010). The membrane was blocked with 5% bovine serum albumin (BSA) for 1 h and incubated with primary antibodies overnight at 4 °C. The membrane was washed 4 times with Tris-buffered saline with 0.1% Tween 20 (TBST), each wash lasting 5 min. The washed membrane was incubated with horseradish peroxidase (HRP)-conjugated secondary antibodies at room temperature for 1 h, washed 4 times with TBST (each wash lasting 8 min), and treated with ECL-enhanced HRP substrate (Proteintech PK10001). Chemiluminescence was detected using a ChemiDoc XRS+ gel imaging system (Bio-Rad). The primary antibodies used were anti-BRD4 (1:3000 dilution, CST#13440), anti-BRD3 (1:100 dilution, Santa Cruz sc-81202), anti-BRD2 (1:3000 dilution, NatureBios A95996), anti-c-myc (1:3000 dilution, Abmart T55150), anti-PARP (1:3000 dilution, Abmart T40050), anti-Bcl-2 (1:5000 dilution, NatureBios A62290), and anti-β-actin (1:5000 dilution, Proteintech 81115-1-RR). The secondary antibodies were HRP-conjugated Goat anti-Rabbit IgG (H + L) (ABclonal, AS014, 1:10 000); HRP-conjugated Goat anti-Mouse IgG (H + L) (ABclonal, AS003, 1:10 000). The markers used were SmartBuffer prestained protein ladder (N6619, 10−250 kDa) or Vazyme 250 kDa plus protein marker (MP201).

Cell Viability and Proliferation Assay. 22RV1, HeLa, U87MG, SK-OV-3, 293T, and RWPE-1 cells were seeded in 96-well plates at a density of 3×10^3 per well. After overnight culture, cells were treated with compounds or a DMSO control (Sigma, USA) for 72 h. The viable cells in the 96-well plate were counted using the Cell Counting Kit-8 (CCK-8) assay (Beyotime, #C0038). The IC_{50} was profiled using GraphPad Prism 9.4.1.

In Vivo Biodistribution. All of the animal studies were performed under the protocol (WP20210588) approved by the Institutional Animal Care and Use Committee of Wuhan University, in accordance with the guidelines of the Chinese Regulations for the Administration of Affairs Concerning Experimental Animals. All mice were purchased from Liaoning Changsheng Biotech Co. Ltd., China. To inoculate tumor cells, trypsinized HeLa, U87MG, or 22RV1 cells were washed twice with RPMI 1640 and resuspended in a 1:1 mixture of RPMI 1640 and Matrigel (Corning). Cells (8×10^6) were implanted subcutaneously into the dorsal region of 6-week-old male BALB/c-nu mice. Tumor volumes and body weights were measured 3 times per week. Tumor volumes were calculated as per the formula [length/2] × [width^2]. The biodistribution study was performed when the tumor volume reached 400 mm^3. SMDC2 (sulfo-Cy5.5 labeled, 100 nmol/kg), SMDC3 (sulfo-Cy5.5 labeled, equal dye dose), and SMDC4 (sulfo-Cy5.5 labeled, equal dye dose) were injected into mice via the tail vein with a volume of 150 μL. Mice were then imaged using the Extreme-II in vivo imaging system (Bruker Xtreme BI) at selected time points (2, 6, 24, 36, 48, and 72 h). At the end of the experiment, the mice were euthanized. The tumors and major organs (heart, liver, spleen, lung, kidney, intestine) were harvested and imaged.

Pharmacokinetic Studies. For pharmacokinetic studies, BALB/C mice (male, ordered from Liaoning Changsheng Biotech) were injected with either SMDC2 (sulfo-Cy7 labeled, 150 nmol/kg) or SMDC3 (sulfo-Cy7 labeled, equal dye dose) bioconjugates. Approximately 30 μL of blood was collected via posterior orbital venous plexus at selected time points (0.3, 1, 2, 4, 6, 8, 12, 24, 48, 72, 96, and 120 h). The fluorescence remaining in blood samples was imaged and quantified using an Odyssey CLx imaging system (LI-COR Biosciences). The pharmacokinetic analysis was performed using Phoenix WinNonlin version 8.1.

Antitumor Therapy in Mice. The xenograft models were established by injection of HeLa (5×10^6), U87MG (6×10^6), or 22Rv1 (5×10^6) cells in 1:1 mixture of RPMI 1640 and Matrigel subcutaneously to the dorsal region of the 6-week-old BALB/c nude mice (male, purchased from Liaoning Changsheng Biotech). When the average tumor volume reached approximately 100 mm^3, the mice were selected based on tumor volume and randomly assigned to groups of 5 animals per group. The compounds SMDC2, SMDC3, and SMDC4, GNE-987 were dissolved in the PBS vehicle containing 5% (v/v) DMSO. The designated drug was then administered via tail-vein injection or subcutaneously (SMDC4 in 30% PF127, v/v = 1:1). PBS 5% containing DMSO served as the vehicle control. The dose regimen and administration route were assigned according to the experiment purpose. During the whole experimental period, both tumor dimensions and mouse body weights were meticulously measured. Tumor volumes and body weights were measured 2−3 times per week, and tumor volumes were calculated as per the formula [length/2] × [width^2].

Immunochemical Analysis of BRD4 Degradation in Tumor Sections. To verify the duration of BRD4 protein degradation in vivo, the tumor-bearing mice were treated with SMDC4 at a single dose of 6 mg/kg. At selected time points (Day 0−14) after treatment, the tumors were harvested, fixed, and paraffin sectioned as above. The BRD4 protein in sections was stained with an anti-BRD4 antibody (1:1000 dilution, CST no. 13440) for histochemical analysis.

Biolayer Interferometry (BLI) Assay. BLI analysis was performed at 30 °C using a ForteBio Octet Red96e biosensor system (ForteBio, Germany) with Amine Reactive Second-Generation (AR2G) Biosensors. For the immobilization of proteins on biosensors, the AR2G biosensors were initially activated with EDC and sulfo-NHS for 5 min. Recombinant human serum albumin (25 μg/mL) was immobilized on the AR2G biosensor for another 5 min. The immobilization reaction was quenched with 1 M ethanolamine for 5 min, and the tips were washed with the kinetics buffer for 10 min to obtain a baseline reading. Thereafter, the biosensors were dipped into wells containing the various concentrations of SMDC1 (from 100 to 3000 nM), SMDC2 (from 100 to 3000 nM), SMDC3 (from 100 to 3000 nM) or SMDC4 (from 100 to 3000 nM) for 3 min, which was followed by a 5 min buffer wash to allow the dissociation of molecules from the sensor. The data were analyzed using ForteBio Data Analysis 11.1 software with a standard 1:1 binding model.

Statistical Analysis. The mean ± standard deviation (SD) was used to report all data. GraphPad Prism software was used to conduct the statistical comparisons using Student's t test as $^*P < 0.05$, $^{**}P < 0.01$. A difference of $^*P < 0.05$ was considered significant.

■ ASSOCIATED CONTENT

Supporting Information

The Supporting Information is available free of charge at https://pubs.acs.org/doi/10.1021/acs.jmedchem.5c00862.

HPLC traces of the SMDC cleavage; IC_{50} profiles; in vivo images of SMDC3 in HeLa tumor xenografts; raw western blotting images; and NMR, mass, and HPLC spectra of key compounds (PDF)

Molecular formula string (CSV)

■ AUTHOR INFORMATION

Corresponding Author

Wanyi Tai − *Department of Pharmaceutical Engineering, School of Pharmaceutical Sciences, Wuhan University, Wuhan, Hubei 430071, China;* orcid.org/0000-0003-3589-8263; Email: wanyi-tai@whu.edu.cn

Authors

Shiwei Song − *Department of Pharmaceutical Engineering, School of Pharmaceutical Sciences, Wuhan University, Wuhan, Hubei 430071, China*

Weina Jing − *Department of Pharmaceutical Engineering, School of Pharmaceutical Sciences, Wuhan University, Wuhan, Hubei 430071, China*

Lei Peng − *Department of Pharmaceutical Engineering, School of Pharmaceutical Sciences, Wuhan University, Wuhan, Hubei 430071, China*

https://doi.org/10.1021/acs.jmedchem.5c00862
J. Med. Chem. XXXX, XXX, XXX−XXX

Jiaqi Liu − *Department of Pharmaceutical Engineering, School of Pharmaceutical Sciences, Wuhan University, Wuhan, Hubei 430071, China*

Complete contact information is available at: https://pubs.acs.org/10.1021/acs.jmedchem.5c00862

Author Contributions

The manuscript was written through contributions of all authors. All authors have given approval to the final version of the manuscript.

Notes

The authors declare no competing financial interest.

■ ACKNOWLEDGMENTS

This work was financially supported by the National Key R&D Program of China (Grant No. 2021YFA0909900) and the National Natural Science Foundation of China (Grant No. 82273860).

■ ABBREVIATIONS USED

ADC, antibody−drug conjugate; BET, bromo and extra-terminal proteins; BLI, biolayer interferometry; BRD4, bromodomain containing protein 4; CBB, Coomassie brilliant blue; DAC, degrader−antibody conjugate; GLP-1, glucagon-like peptide 1; HSA, human serum albumin; iv, intravenous; PK, pharmacokinetic; POI, protein of interest; PROTAC, proteolysis-targeting chimera; RP-HPLC, reversed-phase high-performance liquid chromatography; SAR, structure−activity relationship; sc, subcutaneous injection; SMDC, small molecule−degrader conjugate

■ REFERENCES

(1) Gao, H.; Sun, X.; Rao, Y. PROTAC Technology: Opportunities and Challenges. *ACS Med. Chem. Lett.* **2020**, *11* (3), 237−240.
(2) Miletić, N.; Weckesser, J.; Mosler, T.; Rathore, R.; Hoffmann, M. E.; Gehrtz, P.; Schlesiger, S.; Hartung, I. V.; Berner, N.; Wilhelm, S.; et al. Workflow for E3 Ligase Ligand Validation for PROTAC Development. *ACS Chem. Biol.* **2025**, *20* (2), 507−521.
(3) Chen, S.; Mao, Q.; Cheng, H.; Tai, W. RNA-Binding Small Molecules in Drug Discovery and Delivery: An Overview from Fundamentals. *J. Med. Chem.* **2024**, *67* (18), 16002−16017.
(4) Alugubelli, Y. R.; Xiao, J.; Khatua, K.; Kumar, S.; Sun, L.; Ma, Y.; Ma, X. R.; Vulupala, V. R.; Atla, S.; Blankenship, L. R.; et al. Discovery of First-in-Class PROTAC Degraders of SARS-CoV-2 Main Protease. *J. Med. Chem.* **2024**, *67* (8), 6495−6507.
(5) Pillow, T. H.; Adhikari, P.; Blake, R. A.; Chen, J.; Del Rosario, G.; Deshmukh, G.; Figueroa, I.; Gascoigne, K. E.; Kamath, A. V.; Kaufman, S.; et al. Antibody Conjugation of a Chimeric BET Degrader Enables in vivo Activity. *ChemMedChem* **2020**, *15* (1), 17−25.
(6) Hong, K. B.; An, H. Degrader−Antibody Conjugates: Emerging New Modality. *J. Med. Chem.* **2023**, *66* (1), 140−148.
(7) Zheng, N.; Shabek, N. Ubiquitin Ligases: Structure, Function, and Regulation. *Annu. Rev. Biochem.* **2017**, *86*, 129−157.
(8) Mangano, K.; Guenette, R. G.; Hill, S.; Li, S.; Liu, J. J.; Nadel, C. M.; Archunan, S.; Sadhukhan, A.; Kapoor, R.; Yang, S. W.; et al. VIPER-TACs leverage viral E3 ligases for disease-specific targeted protein degradation. *Cell Chem. Biol.* **2025**, *32* (3), 423−433.
(9) Hoegenauer, K.; An, S.; Axford, J.; Benander, C.; Bergsdorf, C.; Botsch, J.; Chau, S.; Fernández, C.; Gleim, S.; Hassiepen, U.; et al. Discovery of Ligands for TRIM58, a Novel Tissue-Selective E3 Ligase. *ACS Med. Chem. Lett.* **2023**, *14* (12), 1631−1639.
(10) Li, Y.; Wu, Y.; Gao, S.; Sun, T.; Jiang, C. PROTAC delivery in tumor immunotherapy: Where are we and where are we going? *J. Controlled Release* **2025**, *378*, 116−144.
(11) Dragovich, P. S.; Pillow, T. H.; Blake, R. A.; Sadowsky, J. D.; Adaligil, E.; Adhikari, P.; Bhakta, S.; Blaquiere, N.; Chen, J.; dela Cruz-Chuh, J.; et al. Antibody-Mediated Delivery of Chimeric BRD4 Degraders. Part 1: Exploration of Antibody Linker, Payload Loading, and Payload Molecular Properties. *J. Med. Chem.* **2021**, *64* (5), 2534−2575.
(12) Maneiro, M.; Forte, N.; Shchepinova, M. M.; Kounde, C. S.; Chudasama, V.; Baker, J. R.; Tate, E. W. Antibody−PROTAC Conjugates Enable HER2-Dependent Targeted Protein Degradation of BRD4. *ACS Chem. Biol.* **2020**, *15* (6), 1306−1312.
(13) Chan, K.; Sathyamurthi, P. S.; Queisser, M. A.; Mullin, M.; Shrives, H.; Coe, D. M.; Burley, G. A. Antibody-Proteolysis Targeting Chimera Conjugate Enables Selective Degradation of Receptor-Interacting Serine/Threonine-Protein Kinase 2 in HER2+ Cell Lines. *Bioconjugate Chem.* **2023**, *34* (11), 2049−2054.
(14) Chen, Y.; Tandon, I.; Heelan, W.; Wang, Y.; Tang, W.; Hu, Q. Proteolysis-targeting chimera (PROTAC) delivery system: advancing protein degraders towards clinical translation. *Chem. Soc. Rev.* **2022**, *51* (13), 5330−5350.
(15) van Dongen, G. A. Improving Tumor Penetration of Antibodies and Antibody-Drug Conjugates: Taking Away the Barriers for Trojan Horses. *Cancer Res.* **2021**, *81* (15), 3956−3957.
(16) Chames, P.; Van Regenmortel, M.; Weiss, E.; Baty, D. Therapeutic antibodies: successes, limitations and hopes for the future. *Br. J. Pharmacol.* **2009**, *157* (2), 220−233.
(17) Fallah, J.; Agrawal, S.; Gittleman, H.; Fiero, M. H.; Subramaniam, S.; John, C.; Chen, W.; Ricks, T. K.; Niu, G.; Fotenos, A.; et al. FDA Approval Summary: Lutetium Lu 177 Vipivotide Tetraxetan for Patients with Metastatic Castration-Resistant Prostate Cancer. *Clin. Cancer Res.* **2023**, *29* (9), 1651−1657.
(18) Tanyi, J. L.; Randall, L. M.; Chambers, S. K.; Butler, K. A.; Winer, I. S.; Langstraat, C. L.; Han, E. S.; Vahrmeijer, A. L.; Chon, H. S.; Morgan, M. A.; et al. A Phase III Study of Pafolacianine Injection (OTL38) for Intraoperative Imaging of Folate Receptor−Positive Ovarian Cancer (Study 006). *J. Clin. Oncol.* **2023**, *41* (2), 276−284.
(19) Kaur, N.; Popli, P.; Tiwary, N.; Swami, R. Small molecules as cancer targeting ligands: Shifting the paradigm. *J. Controlled Release* **2023**, *355*, 417−433.
(20) Zana, A.; Puig-Moreno, C.; Bocci, M.; Gilardoni, E.; Di Nitto, C.; Principi, L.; Ravazza, D.; Rotta, G.; Prodi, E.; De Luca, R.; et al. A Comparative Analysis of Fibroblast Activation Protein-Targeted Small Molecule−Drug, Antibody−Drug, and Peptide−Drug Conjugates. *Bioconjugate Chem.* **2023**, *34* (7), 1205−1211.
(21) Chen, H.; Liu, J.; Kaniskan, H. Ü.; Wei, W.; Jin, J. Folate-Guided Protein Degradation by Immunomodulatory Imide Drug-Based Molecular Glues and Proteolysis Targeting Chimeras. *J. Med. Chem.* **2021**, *64* (16), 12273−12285.
(22) He, S.; Fang, Y.; Wu, M.; Zhang, P.; Gao, F.; Hu, H.; Sheng, C.; Dong, G. Enhanced Tumor Targeting and Penetration of Proteolysis-Targeting Chimeras through iRGD Peptide Conjugation: A Strategy for Precise Protein Degradation in Breast Cancer. *J. Med. Chem.* **2023**, *66* (24), 16828−16842.
(23) Leamon, C. P.; Vlahov, I. R.; Reddy, J. A.; Vetzel, M.; Santhapuram, H. K. R.; You, F.; Bloomfield, A.; Dorton, R.; Nelson, M.; Kleindl, P.; et al. Folate−Vinca Alkaloid Conjugates for Cancer Therapy: A Structure−Activity Relationship. *Bioconjugate Chem.* **2014**, *25* (3), 560−568.
(24) Luyckx, M.; Votino, R.; Squifflet, J. L.; Baurain, J. F. Profile of vintafolide (EC145) and its use in the treatment of platinum-resistant ovarian cancer. *Int. J. Womens Health* **2014**, *6*, 351−358.
(25) Choi, H. S.; Gibbs, S. L.; Lee, J. H.; Kim, S. H.; Ashitate, Y.; Liu, F.; Hyun, H.; Park, G.; Xie, Y.; Bae, S.; et al. Targeted zwitterionic near-infrared fluorophores for improved optical imaging. *Nat. Biotechnol.* **2013**, *31* (2), 148−153.
(26) Hon, W.-C.; Wilson, M. I.; Harlos, K.; Claridge, T. D. W.; Schofield, C. J.; Pugh, C. W.; Maxwell, P. H.; Ratcliffe, P. J.; Stuart, D. I.; Jones, E. Y. Structural basis for the recognition of hydroxyproline in HIF-1α by pVHL. *Nature* **2002**, *417* (6892), 975−978.

(27) Lewis Phillips, G. D.; Li, G.; Dugger, D. L.; Crocker, L. M.; Parsons, K. L.; Mai, E.; Blättler, W. A.; Lambert, J. M.; Chari, R. V.; Lutz, R. J.; et al. Targeting HER2-positive breast cancer with trastuzumab-DM1, an antibody-cytotoxic drug conjugate. *Cancer Res.* **2008**, *68* (22), 9280−9290.
(28) Song, S.; Liu, Y.; Liu, J.; Tai, W. In silico-driven THIOMAB approach for stable PROTAC conjugates by docking payloads in antibody cavities. *Bioconjugate Chem.* **2025**, *36* (5), 960−970.
(29) Marvin, C. C.; Hobson, A. D.; McPherson, M.; Dunstan, T. A.; Vargo, T. R.; Hayes, M. E.; Fettis, M. M.; Bischoff, A.; Wang, L.; Wang, L.; et al. Self-Immolative Carbamate Linkers for CD19-Budesonide Antibody−Drug Conjugates. *Bioconjugate Chem.* **2023**, *34* (10), 1835−1850.
(30) Ooi, Y. L.; Khang, T. F.; Naidu, M.; Fong, K. C. S. The structural effect of intravitreal Brilliant blue G and Indocyanine green in rats eyes. *Eye* **2013**, *27* (3), 425−431.
(31) Peng, W.; Cotrina, M. L.; Han, X.; Yu, H.; Bekar, L.; Blum, L.; Takano, T.; Tian, G. F.; Goldman, S. A.; Nedergaard, M. Systemic administration of an antagonist of the ATP-sensitive receptor P2 × 7 improves recovery after spinal cord injury. *Proc. Natl. Acad. Sci. U.S.A.* **2009**, *106* (30), 12489−12493.
(32) Georgiou, C. D.; Grintzalis, K.; Zervoudakis, G.; Papapostolou, I. Mechanism of Coomassie brilliant blue G-250 binding to proteins: a hydrophobic assay for nanogram quantities of proteins. *Anal. Bioanal. Chem.* **2008**, *391* (1), 391−403.
(33) Bai, L.; Zhou, B.; Yang, C. Y.; Ji, J.; McEachern, D.; Przybranowski, S.; Jiang, H.; Hu, J.; Xu, F.; Zhao, Y.; et al. Targeted Degradation of BET Proteins in Triple-Negative Breast Cancer. *Cancer Res.* **2017**, *77* (9), 2476−2487.
(34) Lu, J.; Qian, Y.; Altieri, M.; Dong, H.; Wang, J.; Raina, K.; Hines, J.; Winkler, J. D.; Crew, A. P.; Coleman, K.; Crews, C. Hijacking the E3 Ubiquitin Ligase Cereblon to Efficiently Target BRD4. *Chem. Biol.* **2015**, *22* (6), 755−763.
(35) Boulares, A. H.; Yakovlev, A. G.; Ivanova, V.; Stoica, B. A.; Wang, G.; Iyer, S.; Smulson, M. Role of Poly(ADP-ribose) Polymerase (PARP) Cleavage in Apoptosis. *J. Biol. Chem.* **1999**, *274* (33), 22932−22940.
(36) Lau, J.; Bloch, P.; Schäffer, L.; Pettersson, I.; Spetzler, J.; Kofoed, J.; Madsen, K.; Knudsen, L. B.; McGuire, J.; Steensgaard, D. B.; et al. Discovery of the Once-Weekly Glucagon-Like Peptide-1 (GLP-1) Analogue Semaglutide. *J. Med. Chem.* **2015**, *58* (18), 7370−7380.
(37) Bocedi, A.; Cattani, G.; Stella, L.; Massoud, R.; Ricci, G. Thiol disulfide exchange reactions in human serum albumin: the apparent paradox of the redox transitions of Cys(34). *FEBS J.* **2018**, *285* (17), 3225−3237.
(38) Ogitani, Y.; Aida, T.; Hagihara, K.; Yamaguchi, J.; Ishii, C.; Harada, N.; Soma, M.; Okamoto, H.; Oitate, M.; Arakawa, S.; et al. DS-8201a, A Novel HER2-Targeting ADC with a Novel DNA Topoisomerase I Inhibitor, Demonstrates a Promising Antitumor Efficacy with Differentiation from T-DM1. *Clin. Cancer Res.* **2016**, *22* (20), 5097−5108.
(39) Hoogenboezem, E. N.; Duvall, C. L. Harnessing albumin as a carrier for cancer therapies. *Adv. Drug Delivery Rev.* **2018**, *130*, 73−89.
(40) Yu, M.; Benjamin, M. M.; Srinivasan, S.; Morin, E. E.; Shishatskaya, E. I.; Schwendeman, S. P.; Schwendeman, A. Battle of GLP-1 delivery technologies. *Adv. Drug Delivery Rev.* **2018**, *130*, 113−130.
(41) Jing, W.; Peng, L.; Song, S.; Liu, J.; Tai, W. A New Protractor Potentiates Glucagon-Like Peptide 1 with Slow-Release Depot and Long-Term Action. *J. Med. Chem.* **2025**, *68*, 7341−7352.
(42) Yamasaki, K.; Chuang, V. T. G.; Maruyama, T.; Otagiri, M. Albumin−drug interaction and its clinical implication. *Biochim. Biophys. Acta, Gen. Subj.* **2013**, *1830* (12), 5435−5443.
(43) Kawai, A.; Yamasaki, K.; Otagiri, M.; Doi, Y. Interaction of Cephalosporins with Human Serum Albumin: A Structural Study. *J. Med. Chem.* **2024**, *67* (16), 14175−14183.
(44) Rautio, J.; Meanwell, N. A.; Di, L.; Hageman, M. J. The expanding role of prodrugs in contemporary drug design and development. *Nat. Rev. Drug Discovery* **2018**, *17* (8), 559−587.
(45) Huang, W.; Wu, X.; Gao, X.; Yu, Y.; Lei, H.; Zhu, Z.; Shi, Y.; Chen, Y.; Qin, M.; Wang, W.; Cao, Y. Maleimide−thiol adducts stabilized through stretching. *Nat. Chem.* **2019**, *11* (4), 310−319.
(46) Ossipov, D. A.; Gustafsson, O.; Lüchow, M.; El Andaloussi, S.; Malkoch, M. Combination of Coordination and Releasable Covalent Binding for the Delivery of Antisense Therapeutics by Bisphosphonate-Hyaluronan-Oligonucleotide Conjugates. *ACS Appl. Polym. Mater.* **2021**, *3* (4), 2197−2210.

https://doi.org/10.1021/acs.jmedchem.5c00862
J. Med. Chem. XXXX, XXX, XXX−XXX